Evaluating real-time particulate matter instruments against gravimetric and size-resolved references to advance residential wood heater development

Vi H. Rapp[a,*], Brett C. Singer[a], Rebecca Trojanowski[b], Sharon S. Chen[a], Dylan Anacleto-Black[a], William W. Delp[a], Eric Adair[c], John Crouch[c]

[a] *Energy Technologies Area, Lawrence Berkeley National Laboratory, Berkeley CA, United States*
[b] *Interdisciplinary Science Department, Brookhaven National Laboratory, Upton NY, United States*
[c] *Hearth, Patio and Barbecue Association, Arlington, VA, United States*

Abstract

Residential wood heater certification testing relies on time-integrated gravimetric filters that obscure the transient particulate matter (PM) generation events central to heater development. Continuous PM instruments could support advancement of heater technologies, but most are developed for ambient air and may struggle under the high concentrations, dynamic transients, and variable aerosol properties of wood combustion. This study evaluated five continuous PM instruments spanning light scattering (TSI DustTrak II 8530, Thermo MIE pDR-1500, Particles Plus 8306), inertial mass (Thermo Scientific 1405-D TEOM), and triboelectric charge (Sintrol S203) against gravimetric filters and size-resolved reference concentrations across three heater types and two operating phases. No single instrument performed well across all conditions. The DustTrak II and pDR-1500 demonstrated the most consistent temporal tracking ($r \geq 0.87$ and $r \geq 0.79$, respectively) but substantially overestimated integrated PM mass during cordwood combustion and require gravimetric correction for quantitative use. The TEOM performed closest to the gravimetric reference during pellet high-burn phases but exhibited sustained negative cumulative mass during cordwood tests. The Particles Plus and Sintrol showed the weakest overall performance across all conditions. These results support the continued advancement of residential wood heater technologies by identifying conditions under which each instrument provides more or less reliable PM data, and may help inform instrument selection for laboratory testing for product development and field studies for verification.

Keywords: wood smoke aerosol, TEOM, optical particle counter, triboelectric monitor, biomass combustion, light-scattering photometer

*Corresponding author: vhrapp@lbl.gov

1. Introduction

Globally, domestic biomass combustion continues to be an essential residential heating method. With tens of millions of households across the United States and Europe relying on wood for primary or secondary heating, successive generations of heater design have substantially reduced particulate matter (PM) generation over the past decade [11, 16, 34, 65, 69, 70]. As manufacturers refine heater designs and regulators develop certification frameworks that reflect real-world operation, continued advancement of residential wood heating technologies requires measurement tools capable of resolving the transient combustion events that may increase PM generation. Time-integrated gravimetric methods, which have served as the cornerstone of international certification testing for approximately four decades, do not provide this temporal resolution and instead average transient events into a single cumulative value [6–10, 18, 21, 25, 55, 60, 71].

To capture transient PM events, EPA ALT-140, an alternative certification test method, incorporates a continuous PM mass instrument during certification [71]. This method utilizes a Tapered Element Oscillating Microbalance (TEOM) to measure PM mass directly from the dilution tunnel at 1-minute intervals [71]. While the TEOM can log data at 10-second intervals, it is subject to signal noise that can reduce precision [61, 62]. Furthermore, the instrument is bulky, expensive, and faces operational challenges in combustion environments [2, 4, 20, 30, 32, 39, 56, 61]. For instance, its collection filters are prone to rapid overloading under heavy particulate loads, requiring multiple manual filter changes within a single test cycle [2, 33, 35, 61]. The heated sensor element can also trigger volatilization of semi-volatile compounds or experience mechanical shedding from filter oscillation under dynamic flows, leading to significant measurement fluctuations [4, 22, 39, 42, 54]. Although the instrument has proven viable for laboratory testing of wood heaters, studies using the TEOM with wood heaters in the field are limited [39, 56, 75]. Also, the manufacturer announced that production of the TEOM is ending, with no orders accepted after June 30, 2026.

Integrating portable, continuous PM measurements could enhance wood heater designs while expanding understanding of wood heater performance in the laboratory and the field. However, the vast majority of continuous PM instruments are designed for ambient conditions with low mass concentrations and stable, near-ambient temperatures [4, 61, 62]. Wood combustion exhaust, by contrast, presents a harsh, high-concentration environment (>400 mg/m^3 when sampling from the dilution tunnel) that can challenge the operation and measurement range of many PM instruments.

Light-scattering instruments offer an appealing alternative to the TEOM due to their portability and ease of use [1, 32, 58]. Yet, their application to wood heater testing is complicated by aerosol morphology [1, 28, 46]. A substantial portion of the PM generated during wood combustion consists of particles smaller

than 300 nm in diameter [14, 15, 19, 26, 66]. Because many portable optical monitors have an effective lower detection limit of about 100–300 nm, they can significantly underpredict total mass [1, 28, 46, 58, 75]. Factory-calibrated scaling algorithms can partially compensate, but they frequently fail to account for the unique refractive indices of wood smoke and shifts in the sub-300 nm particle fraction across combustion conditions [67]. Conversely, some monitors may overcompensate via these internal algorithms, leading to overprediction during peak events [1, 46, 58]. While co-located gravimetric filters can be used to calibrate these optical responses, performing continuous filter corrections adds a substantial operational burden during in-home field studies [76, 77].

To avoid filter loading and dilution complexities associated with TEOMs and light-scattering instruments, some PM monitors can track particles directly from the undiluted exhaust stack. For example, opacity sensors use light extinction to handle high-concentration pathways through direct visual attenuation [50, 53, 64]. Some specialized devices are designed to monitor particulate output directly from the chimney, while other industrial monitors offer rugged designs that could be adapted to wood heaters [50, 53]. However, many industrial opacity sensors require long physical path lengths to maintain measurement sensitivity, and they require empirical calibrations to correlate raw opacity data to true PM mass [52, 64]. Similarly, triboelectric monitors offer a rugged, filterless option for direct stack monitoring [24, 43]. Yet, their sensitivity to particle charge, exhaust velocity, and composition variations remains poorly characterized under transient operational phases [24]. Consequently, while both opacity and triboelectric instruments allow for direct exhaust measurements, these options may be better suited for tracking relative PM trends rather than providing real-time PM mass concentrations across laboratory and field settings.

The purpose of this paper is to (1) assess if any real-time instrument(s) could replace the integrated gravimetric filter as the basis for a certification mass measurement; (2) determine if any instrument(s) can provide time-resolved information to support heater design and combustion research; and (3) explore the implications of these laboratory findings for assessing in-home performance. To achieve these goals, we evaluate five real-time PM instruments for measuring wood heater PM across three heater types and two operational phases. The instruments span three measurement principles: light-scattering (DustTrak II 8530, MIE pDR-1500, and Particles Plus 8306), inertial mass measurement (TEOM 1405-D), and triboelectric (Sintrol S203). Each instrument is evaluated during startup, high-burn, and low-burn phases of three residential room heater types (non-catalytic cordwood, catalytic cordwood, and pellet), with performance benchmarked against laboratory-grade gravimetric and size-resolved shape reference. Integrated mass measured by each instrument was compared with the gravimetric reference, while temporal tracking of the PM measurements were compared with the size-resolved shape reference. By identifying which instruments reliably provide integrated mass measurements and resolve transient PM events across heater types and operating phases,

this work supports the measurement infrastructure needed for continued advancement of residential wood heater technology.

2. Methods

2.1. Experimental Setup

Exhaust from the heaters was captured and diluted using a dilution tunnel system compliant with ASTM E2515-11 [5]. To minimize particle losses, PM was sampled using a seamless, stainless-steel bent probe nozzle recommended by EPA Method 5, instead of a straight sampling probe [72]. Dilution tunnel flow rates were verified using a standard Pitot tube, and set to approximately 14.15 m^3/min (∼500 SCFM) for cordwood heaters and 8.5 m^3/min (∼300 SCFM) for the pellet heater. All dilution tunnel and sampling flow rates were measured and maintained at standard conditions (25 °C and 101.325 kPa), and reported PM mass concentrations (mg/m^3) reflect standard temperature and pressure. Type T exposed-junction thermocouples measured dilution tunnel, ambient, and gravimetric sampling train temperatures, and an Omega RH-USB sensor measured dilution tunnel relative humidity. Exhaust gas concentrations of carbon monoxide (CO) and carbon dioxide (CO_2) were recorded from the dilution tunnel to track real-time dilution ratios and calculate modified combustion efficiency (Section S-2.6). All instrument outputs were displayed and logged using a custom Python-based program. A schematic of the dilution tunnel system is shown in Figure 1.

A secondary dilution system kept sample concentrations within optimal instrument ranges and prevented fouling by blending controlled flows of dilution tunnel aerosol and ultra-zero grade air from a gas cylinder. The ultra-zero air met the following specifications: O_2 19.5–23.5%, water < 2 ppm, hydrocarbons < 0.1 ppm, $CO_2 < 0.5$ ppm, and CO < 0.5 ppm. The effective dilution factor was tracked in real time by comparing CO_2 measurements in the secondary dilution line (PP Systems SBA-5 nondispersive infrared (NDIR)-CO_2 analyzer) to those in the dilution tunnel (California Analytical Instruments 600 Series NDIR analyzer). Gas analyzers were zeroed and spanned at the start of each test day and zero-checked at the end of each test day. Secondary dilution ranges for each phase are summarized in Table S1. Particle transport losses through the secondary dilution line were evaluated using the Particle Loss Calculator [78]. For the primary mass-bearing size range of wood smoke aerosol (0.03–2.5 μm), estimated combined penetration efficiency through the secondary dilution manifold exceeded 95%, indicating negligible sampling line losses prior to instrument detection.

2.2. Heater Specifications

Experiments were conducted with three wood heaters: a catalytic cordwood heater (Blaze King Sirocco SC20.2), a non-catalytic cordwood heater (Quadra-Fire 4300 Millennium), and a pellet heater (Regency

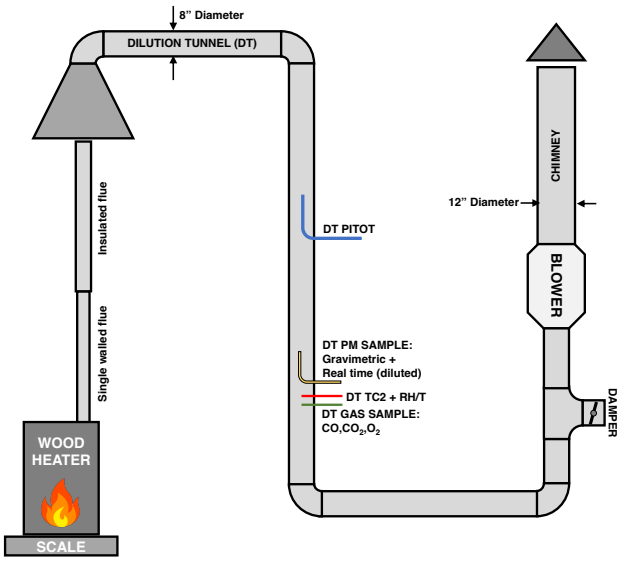


Figure 1: Schematic of laboratory experimental setup with dilution tunnel (DT). Note: TC is thermocouple, P is pressure, and PM is particulate matter.

Greenfire GF55) [13, 48, 51]. EPA certification test results for each heater can be found in the EPA Certified Wood Heater Database [73]. The catalytic cordwood heater has a 1.8 cu. ft (0.051 cu. m) firebox and was acquired new in 2023. The catalytic combustor is located at the top of the firebox (combustion-chamber outlet), and exhaust gases are routed through the catalyst when the bypass damper is closed [13]. Specific active phase compositions and substrate geometries are proprietary to the manufacturer. The non-catalytic cordwood heater has a 2.3 cu. ft (0.065 cu. m) firebox and was obtained used from the manufacturer following quality control testing in 2025. The pellet heater was purchased new in 2024. Prior to use in these experiments, each heater was pre-conditioned by undergoing at least 48-hours of operation at medium-to-high burn rates. Each heater was installed with a chimney stack following standard laboratory test methods [6–9]; details about the chimney materials and heights are provided in Section S-1.2.

2.2.1. Heater Operation

Each heater was operated in two phases: a *high-burn* phase, capturing cold (room-temperature) startup through steady-state operation at near-maximum burn rates, and a *low-burn* phase, capturing turndown through steady-state operation at near-minimum burn rates. Two replicate tests were conducted for each heater and phase, for a total of 12 tests. Initial conditions, heater settings, and key events for each phase

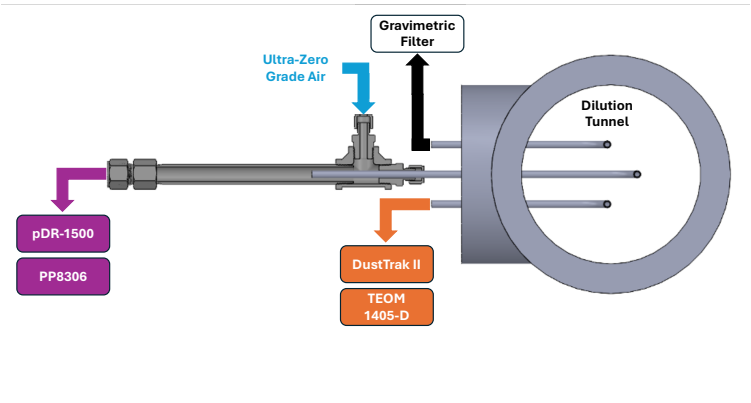


Figure 2: Cross-sectional schematic of 90° bent-sampling probes viewed from the bottom of the dilution tunnel, and the secondary dilution system to PM instruments.

are provided in Section S-1.3. Consistent with certification practice, burn phases are defined by the firebox initial conditions: a high-burn phase begins from a cold (room-temperature) firebox and a low-burn phase begins from a hot coal bed. Because each phase is established by these initial conditions, more than one phase may be conducted on a single test day.

The high-burn phase for the cordwood heaters begins with ignition of paper, kindling, and small logs in a cold firebox with air controls set to maximum (∼10–20 minutes). A charge of two to five larger logs is added once the firebox is hot. For the catalytic cordwood heater, the catalyst is engaged immediately after loading this charge. The heater then operates at high output for the remainder of the phase. The pellet heater's high-burn phase includes an automated 10–15 minute startup sequence initiated when the heater is powered on. After startup, it operates at 'Heat Level 5' for the remainder of the phase.

The low-burn phase for the cordwood heaters begins with a fresh reload of 2–3 larger logs, after which the burn rate controls are reduced to their low-burn settings. The non-catalytic cordwood heater has an Automatic Combustion Control (ACC) in addition to a burn rate lever. The ACC provides additional combustion air that is automatically controlled over approximately 25 minutes to quickly ignite new logs. The manual recommends engaging the ACC right before adding fuel. It should be noted that during the second low-burn test, the ACC was engaged about 5-minutes after loading the fuel, which increased PM generation. Burn rate for the catalytic cordwood heater is reduced manually by stepping down the thermostat adjustment twice over the first 10 minutes. Each phase continues until less than 1.0 kg of fuel (based on the scale reading) remains in the firebox. The pellet heater's low-burn phase begins when the operator selects Heat Level 2. The heater automatically reduces the pellet feed rate and operates at steady-state for approximately 2 hours, after which it is powered off. The final 10 minutes of the low-burn phase captures a portion of the heater's automated shutdown sequence, in which all remaining pellets in the burn-pot are extinguished. This corresponds to the first 10 minutes of the 40-minute shutdown sequence outlined in the

certification test.

All heaters were fueled with Douglas fir, which was selected to align with fuel species used during U.S. EPA wood heater certification testing [8, 9, 18]. Seasoned cordwood was sourced locally in 2023 and pellets purchased in 2020. The dry fuel consumption during each heater operating phase is reported in Table 1. Additional details about the fuel, including composition and moisture content, can be found in Section S-1.4.

Table 1: Dry fuel consumed in kilograms for each heater by test phase. Two replicate tests were conducted for each heater and each operating phase.

Phase	Test	Non-Cat Cordwood (kg)	Cat-Cordwood (kg)	Pellet (kg)
High-burn	1	7.1	3.3	2.1
	2	4.9	3.3	2.1
Low-burn	1	1.2	2.3	2.1
	2	1.3	2.8	2.0

2.3. Reference Particle Methods

To evaluate the accuracy and temporal response of the five PM instruments, their cumulative mass and real-time measurements were compared against two references: a gravimetric filter measurement and reconstructed mass concentration derived from three particle size spectrometers spanning 5.6 nm to 20 µm.

The reference cumulative PM mass for each phase was determined gravimetrically using a modified version of test method ASTM E2515-11 [5]. Exhaust from the dilution tunnel was sampled iso-axially through a filter train containing two pre-weighed 47 mm PTFE-bonded glass fiber filters (Cytiva Pallflex Emfab™) mounted in series. PTFE-bonded glass-fiber filters were selected to minimize fiber loss during handling while providing comparable PM measurements to the binder-free glass-fiber filters specified in North American standards [3, 7–9, 21, 74]. A single gravimetric filter train was deployed per operational phase and filters were replaced prior to each phase to ensure each integrated mass measurement corresponded to a single phase. For the non-catalytic cordwood heater, all instrument sampling was stopped about 15 minutes after startup to replace the reference filter and the DustTrak II filter. This was necessary to prevent filter overloading and about 5-minutes of startup data was not recorded. After the filters were replaced, instrument sampling resumed and the high-burn logs were added into the firebox. Flow rates across the filter train were held constant at about 3 liters per minute (LPM) for all operating phases except for the second low-burn phase of the non-catalytic cordwood heater, which was held constant at 6 LPM. The flow rate for this phase was increased to ensure filter masses would exceed the minimum accuracy of the microbalance.

The net catches from the two cordwood high-burn filter trains were summed to yield a single integrated startup-plus-high reference mass, consistent with the single-filter treatment of the catalytic cordwood and

pellet high-burn phases. Gravimetric filters were desiccated at room temperature before and after sampling in accordance with ASTM E2515-11 [5]. Pre- and post-test filter weights were measured on an ultramicrobalance. Cumulative PM mass for each phase was calculated as the sum of net catches on both filters. Filter holders, gaskets, and probes were flushed at the start and inspected at the end of each test day; PM deposition on these surfaces was visually confirmed to be negligible and was not quantified.

The reference real-time mass concentration (hereon referred to as the size-resolved shape reference) was reconstructed from three particle size spectrometers: a TSI 3321 Aerodynamic Particle Sizer (APS), TSI 3330 Optical Particle Sizer (OPS), and TSI 3091 Fast Mobility Particle Sizer (FMPS). Together, these instruments measured particle number concentration from 6 nm to 20 µm at 1 Hz, spanning a size range no single instrument covers. To prevent double-counting in regions of overlapping detection, bins at the edges of each instrument's range were excluded. The FMPS contributed bins below 300 nm, the OPS bins from 300 to 700 nm, and the APS bins above 700 nm, with each boundary assigned to a single instrument. Time-resolved particle counts were converted to mass concentration using per-phase effective densities derived from the gravimetric filter measurements (see Section 2.5). All three instruments sampled from the secondary dilution line (Figure 2) and were zeroed with Ultra-Zero grade air at the start of each test day. Further details on the FMPS, OPS, and APS are provided in Section S-1.5.

2.4. Particulate Instruments

Five continuous PM instruments were evaluated across three residential wood heater types operating in startup, high, and low-burn phases. Instruments evaluated included light-scattering (TSI DustTrak II 8530, Thermo Scientific MIE pDR-1500, and Particles Plus 8306), inertial mass measurement (Thermo Scientific TEOM 1405-D), and triboelectric (Sintrol S203). Instruments were operated per the manufacturers instructions with the exception of the TEOM. A brief summary of each instrument and how it was operated is provided below. Additional details about each instrument can be found in Section S-2.7.

DustTrak II 8530. The TSI DustTrak II 8530 (DT2) is a single-channel, 90° light scattering, photometric instrument that uses a laser diode to determine the mass concentration of aerosols in real time [67, 68]. Related models in this family include the EP version, which uses an external pump, and the DRX family, which provides multi-channel mass fraction reporting. According to specifications, the DT2 has a concentration range of 0.001 to 400 mg/m^3 and detects particle sizes from 0.1 to 10 µm. The DT2 is calibrated against a reference photometer that is gravimetrically calibrated to ISO 12103-1, A1 ultrafine test dust (Arizona Test Dust). While the raw, A1 dust features a geometric median diameter of approximately 3 to 5 µm, the size-selective aerosolization process utilized during factory calibration isolates a cloud with a mass median aerodynamic particle diameter of 2.5 µm. The instrument software interprets this standard using a blended

material refractive index of 1.51 and assumes a solid particle density of 2.65 g/cm^3 [67, 68]. The test dust consists primarily of silicon dioxide and aluminum oxide, which together account for roughly 80% to 90% of its total mass, supplemented by minor amounts of iron, alkali metals, and alkaline earth metals.

The DT2 features an internal 37 mm filter cassette for concurrent gravimetric sampling, which the manufacturer recommends using to establish aerosol-specific photometric calibration factors. Of the total 3.0 LPM sample flow, two-thirds passes through the internal gravimetric filter as sample flow, with the remaining one-third diverted as sheath flow. The internal flow controller maintains this total flow to within ±5% of the factory set point [68]. The DT2 sampled directly from the dilution tunnel since past experience demonstrated it could recover if concentrations exceeded its maximum limit. The 37 mm filter was replaced at the beginning of each test phase to coincide with the replacement of the 47 mm reference filter, ensuring identical sampling durations for a parallel comparison. Although particle size selection can be performed using optional inlet impactors, no impactors were used in this study. On the morning of each test day, the internal filter elements (sheath air HEPA filters) were replaced, and a zero calibration was performed using an inline HEPA filter. The total flow rate was also confirmed at the beginning of each test day and monitored after each filter change.

MIE pDR-1500. The Thermo Scientific MIE pDR-1500 (pDR) is a nephelometric monitor designed for personal sampling that uses infrared scattering from an 880 nm Light Emitting Diode (LED) to estimate PM mass concentrations [63]. According to its specifications, the pDR has a measurement range of 0.001 to 400 mg/m^3 and responds to an optical particle size range of approximately 0.1 to 10 µm. It is calibrated against a reference monitor that is gravimetrically calibrated to ISO 12103-1, A2 Fine Arizona Test Dust (historically SAE Fine). While the dry test dust possesses a geometric median diameter of approximately 10 µm, the manufacturer notes that upon aerosolization into the instrument's calibration chamber, the floating fraction yields a mass median aerodynamic particle diameter of 2 to 3 µm with a geometric standard deviation of 2.5. The manual also references a calibration material refractive index of 1.54 (corresponding to silicon dioxide) and defines the bulk density as 2.60 to 2.65 g/cm^3 [63].

Downstream of the photometric sensing stage, the monitor incorporates a 37 mm filter holder that protects the pump from any sampled aerosol and serves as a sample collection filter for gravimetric analysis [63]. For this study, the red inlet cyclone (Model GK 2.05) was used at a flow rate of 1.19 LPM, corresponding to an approximate PM_{10} aerodynamic cut point [63]. The pDR sampled from the secondary dilution system (Figure 2) to maintain concentrations within its operating range. At this dilution level, the mass collected on the 37 mm filter fell within the weighing uncertainty of the microbalance, making a meaningful gravimetric comparison with the 47 mm reference filter unreliable. On the morning of each test day, a zero calibration

was completed using an inline HEPA filter. The relative humidity correction was disabled and the calibration factor was set to 1.000.

Particles Plus 8306. The Particles Plus 8306 (PP8306) is an optical particle counter designed to measure real-time particle counts and approximate total mass concentrations from light-scattering data [47]. The handheld instrument utilizes laser diode technology to sample air at a volumetric flow rate of 2.83 LPM controlled by an internal vacuum pump. Operating across a concentration range of 0.01 to 20,000 µg/m^3, the PP8306 sorts detected particles into six size channels ranging from 0.3 to 10.0 µm. To translate these raw optical counts into real-time mass concentrations (µg/m^3), the internal firmware calculates the weight of the sample using the average size of each channel alongside user-defined density and refractive index adjustments. The PP8306 complies with ISO 21501-4 and JIS B9921 standards, and is calibrated using a National Institute of Standards and Technology (NIST) traceable source, typically polystyrene spheres, at specific particle size channels: 0.3, 0.5, 1.0, 2.5, 5.0, and 10.0 µm [31]. The polystyrene spheres typically have an average particle density of 1.05 g/cm^3 and a refractive index of 1.59.

The PP8306 sampled from the secondary dilution system to prevent concentrations from exceeding its operating range. For this study, the mass density for each channel was set to 1.26 g/mL based on previous experiments using Douglas fir and validated with experimental data collected in this study [49]. The refractive index was set to 1.56 matching previous research measuring properties for Douglas fir smoke aerosol [29, 38]. To be consistent with the other instruments, the total PM mass concentration is reported in this study. At the beginning of each test day, a zero-count check was conducted using an inline HEPA filter.

Thermo Scientific TEOM 1405-D. The Thermo Scientific TEOM 1405-D is a dual-channel real-time mass monitor that incorporates two independent tapered element oscillating microbalance systems within a single instrument chassis [62]. Because EPA references two different standard operating procedures for using the TEOM with wood heaters, we followed the newest protocols with minor deviations [45, 71]. Specifically, the impactor was removed for this study so both channels provide the same PM_{Total} measurement, even though the system is designed as a dichotomous monitor to simultaneously isolate and measure $PM_{2.5}$ and PM_{Coarse} fractions using a virtual impactor. This modification allows for side-by-side monitoring to verify data consistency. The internal sample stream heaters were also disconnected [45].

The TEOM sampled directly from the dilution tunnel. Instrument setup, routine operations, and filter handling procedures generally followed the standard operating procedure recommended by EPA [45]. At the beginning of each test day, the TEOM internal clock and data logging configurations were verified. New Pallflex TX40 filter cartridges were installed with a nominal sample flow rate set to 1.00 LPM for the pellet and catalytic-cordwood heaters and 0.50 LPM for the non-catalytic cordwood heater to prevent filter

overloading. The instrument was operated for at least 1 hour, sampling clean air from a flowing dilution tunnel, to allow pressure-related pneumatic transients to fully stabilize. Leak and flow checks were conducted on both channels before installing new filters and immediately following test completion using a certified reference flow meter. Pre-test criteria mandated a leak rate of $\leq$0.10 LPM and flow rate within 2.0% of the setpoint (1.00 LPM), whereas post-test limits were set to $\leq$0.15 LPM for leaks and within 4.0% for flow. A single filter set was used for each test where possible, with replacement occurring before filter loading reached 100% to ensure valid instrument operation and maintain sample flow control [45]. When a filter change was required, the filters on both channels were replaced simultaneously and system stability was verified before resuming collection.

Deviating from the 60-second reporting protocols outlined in the EPA-recommended standard operating procedures, the TEOM data were recorded at 10-second intervals to fully characterize transient operational phases, such as heater startup [45]. At 10-second resolution, each measurement reflects the mass accumulated over a shorter interval, resulting in a lower signal-to-noise ratio and potentially a reduced per-point precision compared to 60-second measurements; however, the cumulative mass and therefore the mean concentration over the same sampling period should be equally accurate [36, 44]. Higher time-resolution data also revealed localized instrument transients such as particle shedding and instantaneous negative mass concentrations that have been observed in previous research [4, 22, 39, 42, 54, 61]. Retaining the negative concentration values was necessary to prevent artificial inflation of the cumulative mass calculation [39]; the older EPA operating procedures also recommend retaining negative measurements [71].

Sintrol S203 Dust Monitor. The Sintrol S203 (Sintrol) is an in-duct dust monitor designed for continuous measurement of total suspended particles (TSP) in industrial process airflows [59]. The instrument operates on the principle of inductive electrification, in which an isolated stainless-steel sensor probe is inserted perpendicular to the airflow; as charged particles pass near the probe, they induce an AC signal that is proportional to dust concentration. According to the manufacturer, the instrument has a detection limit of 0.01 mg/m^3 and responds optimally to particles between 1 and 200 µm. Unlike the photometric instruments described above, converting the inductive signal to a mass concentration requires a material-specific calibration factor that accounts for differences in particle charge generation across dust types, sizes, and flow conditions [24]. The manufacturer states that the signal response is linear up to several hundred mg per cubic meter, beyond which it becomes nonlinear before reaching saturation at several grams per cubic meter [59]. The specifications also note that it has a minimum detectable particle size of 0.3 µm and a minimum recommended duct flow velocity of 3 m/s. Because the S203 does not support entry of a material-specific calibration factor, data were logged in Inductive Electrification Units (IEU) and converted to mass concen-

288 tration in post-processing using the 47 mm gravimetric reference measurements. The Sintrol was installed
289 in the horizontal section of the dilution tunnel after the other PM instruments, located approximately five
290 duct-diameters from the upstream elbow and three duct-diameters from the downstream elbow (see Figure
291 1). The probe extended approximately 6.75 inches (190 mm) into the 8-inch (203 mm) diameter duct and
292 logged data at a 50-second signal averaging interval. At the beginning of each test day, the Sintrol probe was
293 cleaned, proper grounding was confirmed per the manufacturer's instructions, and baseline measurements
294 were collected with the dilution tunnel sampling ambient air [59].

295 *2.5. Data Analysis for Size-Resolved Shape Reference*

296 To calculate the size-resolved mass concentration reference at each time step, $M_{\text{ref}}(t)$, an effective particle
297 density was determined for each phase using an iterative algorithm that reconciled particle size distribution
298 measurements from the FMPS, OPS, and APS with gravimetric filter measurements. The algorithm started
299 by assuming a density of 1.0 g/cm^3 and then converted the FMPS mobility diameters to aerodynamic
300 diameter using

$$d_a = d_m \sqrt{\rho_e / \rho_0} \tag{1}$$

301 where d_a is aerodynamic diameter, d_m is mobility diameter, ρ_e is the effective particle density, and ρ_0 is a
302 unit density (1.0 g/cm^3).

303 Next, the total particle volume across all particle instruments was calculated for a sampling time that
304 matched the gravimetric measurement sampling time. This was done by calculating the total particle number
305 distribution over the course of the test for each particle bin using,

$$N_{\text{test}}[\#] = \sum_{d=d_i}^{d=d_f} \sum_{t=0}^{t_{\text{test}}} \left((dN/d\log D_p)_t \right)_d \left[\frac{\#}{\text{cm}^3} \right] \cdot \bar{Q}_{\text{duct}} \left[\frac{\text{m}^3}{\text{s}} \right] \cdot \Delta t\,[\text{s}] \cdot d\log D_p \cdot \frac{10^6\ \text{cm}^3}{1\ \text{m}^3} \tag{2}$$

306 where t_{test} is the duration of the test in seconds, $\bar{Q}_{\text{duct}}$ is the mean dilution tunnel volumetric flow rate, and
307 Δt is the sampling interval, equal to 1 second for all instruments. Then, the total particle volume during
308 the sampling period was calculated using,

$$V_{\text{test}}\,[\text{cm}^3] = \frac{1}{6}\pi d^3\,[\text{nm}^3] \cdot N_{\text{test}}[\#] \cdot \frac{10^{-21}\ \text{cm}^3}{1\ \text{nm}^3}, \tag{3}$$

309 and the effective density was calculated using,

$$\rho_e \left[\frac{\text{g}}{\text{cm}^3} \right] = \frac{M_{\text{filt}}\,[\text{mg}]}{V_{\text{test}}\,[\text{cm}^3] \cdot \frac{1000\ \text{mg}}{1\ \text{g}}}, \tag{4}$$

where M_{filt} is the total gravimetric mass collected on the filter over the test duration, and V_{test} is the integrated particle volume computed from the three spectrometers.

The calculated ρ_e was compared with the initial guess; if the values differed by more than 0.1%, the updated ρ_e (Equation 4) was used to convert the FMPS mobility diameters to aerodynamic diameters (Equation 1) and the cycle was repeated. Damping (weighted averaging with the previous iteration using $\alpha = 0.5$) and safeguards to detect physically unrealistic density values (≤ 0 or > 20 g/cm^3) were applied to stabilize convergence, with a maximum iteration limit of 1000. The resulting per-phase effective densities are reported in Table S9.

With the effective density converged and the FMPS bin diameters corrected, the total particle number, $dN(t)$, over a specified diameter range was calculated at each time step using,

$$dN(t)\left[\frac{\#}{\text{m}^3}\right] = \sum_{d=d_i}^{d=d_f}\left(\frac{dN(t)}{d\log D_p}\right)_d\left[\frac{\#}{\text{cm}^3}\right]\cdot d\log(D_p)\cdot\frac{10^6\ \text{cm}^3}{1\ \text{m}^3} \tag{5}$$

where $\frac{dN(t)}{d\log D_p}$ is the particle number concentration at time t for geometric mean diameter d, d_f and d_i are the upper and lower bounds of the particle diameter range in nm, and $d\log(D_p)$ is the log (base 10) of the instrument-specific constant bin width. Note that units for each variable are presented in the square brackets.

Next, the total particle volume, $dV(t)$, at a given time was calculated using

$$dV(t)\left[\frac{\text{cm}^3}{\text{m}^3}\right] = \frac{1}{6}\pi d^3\left[\text{nm}^3\right]\cdot dN(t)\left[\frac{\#}{\text{m}^3}\right]\cdot\frac{10^{-21}\ \text{cm}^3}{1\ \text{nm}^3} \tag{6}$$

Then, the total mass concentration, $dM(t)$, at a given time was calculated using

$$dM(t)\left[\frac{\text{mg}}{\text{m}^3}\right] = dV(t)\left[\frac{\text{cm}^3}{\text{m}^3}\right]\cdot\rho_e\left[\frac{\text{g}}{\text{cm}^3}\right]\cdot\frac{1000\ \text{mg}}{1\ \text{g}} \tag{7}$$

To avoid double-counting in the overlapping size ranges of the three spectrometers, the size-resolved shape reference at each timestep was computed as the sum of $dM(t)$ from each instrument over its assigned, non-overlapping diameter range (as described in Section 2.3):

$$M_{\text{ref}}(t) = dM_{\text{FMPS}}(t) + dM_{\text{OPS}}(t) + dM_{\text{APS}}(t), \tag{8}$$

where each instrument's contribution is evaluated over its assigned bin range.

2.6. Gravimetric Correction

For temporal concentration comparisons, all instruments were corrected to the 47 mm gravimetric reference measurement for each operational phase [37, 63, 68]. For each phase, the instrument concentration data were time-averaged over the phase duration, accounting for the secondary dilution factor where applicable. This phase-averaged concentration was then compared to the time-integrated mass concentration derived from the 47 mm gravimetric filter to yield a bulk correction factor. Each discrete data point in the continuous time series was multiplied by this correction factor to produce the final gravimetrically corrected PM mass concentration time series. For the Sintrol, the ambient baseline IEU signal was subtracted from the raw measurements prior to applying the gravimetric correction. The correction factors derived for each instrument and operational phase are reported in Table S8.

2.7. Statistical Analysis

Agreement between each PM instrument and the size-resolved shape reference was assessed using the Pearson correlation coefficient (r), which quantifies the strength and direction of the linear relationship between two variables. The coefficient was calculated between each instrument's time-resolved output and the size-resolved shape reference for each heater and operating phase. The Pearson r was selected over the coefficient of determination (R^2) because its sign carries physically meaningful information, as several instruments returned negative r values during low-burn and pellet phases, indicating an inverse relationship with the reference that would be obscured by squaring. Bland-Altman analysis and parity plots are also provided in the supplemental data to further evaluate systematic bias (median difference) and limits of agreement [12, 27, 40, 41, 57]. Because the data was not normally distributed, limits of agreement were calculated as the 2.5^{th} and 97.5^{th} percentiles rather than the mean $\pm 1.96 \times$SD. All metrics were computed on 10-second averaged data over each operating phase. Prior to all comparative analyses, continuous instrument time series were individually aligned to the size-resolved shape reference to correct for sampling-line and instrument response delays. For each instrument, the time offset relative to the size-resolved reference was estimated by finding the shift that gave the closest alignment between the two mass concentration time series during the high-burn phase. The same offset was then applied across all test phases for that instrument. A time offset was not applied to the Sintrol because its collection frequency was 50-seconds and the triboelectric output was not directly comparable to a mass concentration reference.

3. Results and Discussion

Five continuous PM instruments were evaluated against gravimetric filter and size-resolved reference concentrations across three heater types and two operating phases. Each instrument is assessed in terms of

its agreement with the gravimetric reference measurement, its ability to capture transient PM events, and the practical implications of these findings for field deployment.

3.1. Gravimetric Reference Agreement

Table 2 reports the corresponding time-integrated PM mass from each instrument alongside the reference gravimetric filter and the DT2 onboard gravimetric filter. Figure 3 shows the mass ratio of each instrument to the gravimetric filter reference for each heater type and operating phase, where ratios greater than 1.0 indicate overestimation (orange) and ratios less than 1.0 indicate underestimation (purple). Phases where the instrument reported a negative cumulative mass are excluded from the ratio comparison. No correction factors are applied to the real-time instrument data, and secondary dilution is accounted for where applicable (see Section 2.1). The Sintrol is excluded from this comparison because its triboelectric TSP output could not be converted to a total PM mass without using the gravimetric filter measurement.

Table 2: Integrated PM mass from the gravimetric filter reference, the DustTrak II gravimetric filter (DT2 Grav), and time-integrated PM from the DustTrak II (DT2), pDR1500 (pDR), Particles Plus 8306 (PP8306), and both channels of the TEOM across all heater types and operating phases. All reported masses are in grams. pDR data was not collected for three of the non-catalytic cordwood tests due to user error. Note that the automatic air control for the second low-burn test for the non-catalytic cordwood heater was engaged late, leading to higher particulate matter generation than the first test.

Heater	**Phase**	**Reference**	**DT2 Grav**	**DT2**	**pDR**	**PP8306**	**TEOM A**	**TEOM B**
Non-Catalytic Cordwood	High 1	6.00	5.43	11.77	2.34	1.98	5.72	5.60
	High 2	6.96	5.68	15.87	—	2.89	5.58	5.60
	Low 1	0.72	0.50	1.01	—	0.36	-0.05	0.05
	Low 2	6.71	4.88	25.45	—	3.40	4.98	4.94
Catalytic Cordwood	High 1	9.87	8.37	34.31	9.56	3.99	-9.49	9.80
	High 2	6.48	5.19	17.68	5.30	3.05	5.61	5.56
	Low 1	1.08	0.74	5.09	1.17	0.93	0.87	-16.81
	Low 2	1.66	1.04	6.15	2.56	1.49	0.76	0.80
Pellet	High 1	2.06	1.85	1.76	0.36	0.20	2.01	1.96
	High 2	1.88	1.88	2.10	0.44	0.16	2.02	2.01
	Low 1	1.22	1.02	0.36	0.09	0.32	0.99	0.97
	Low 2	1.04	0.98	0.37	0.10	0.18	0.57	0.61

DT2 Gravimetric Filter. The onboard gravimetric filter of the DT2 (DT2 Grav) showed generally good agreement with the reference across all heater types and phases, with mass ratios ranging from 0.63 to 1.00, consistently falling at or below unity. The closest agreement occurred during pellet heater operation, with ratios between 0.84 and 1.00 and no clear difference between high- and low-burn phases. Both cordwood heaters showed substantially lower ratios during low-burn (0.63–0.73) compared to high-burn (0.80–0.90), and their high-burn ratios were on average lower than those observed for the pellet heater.

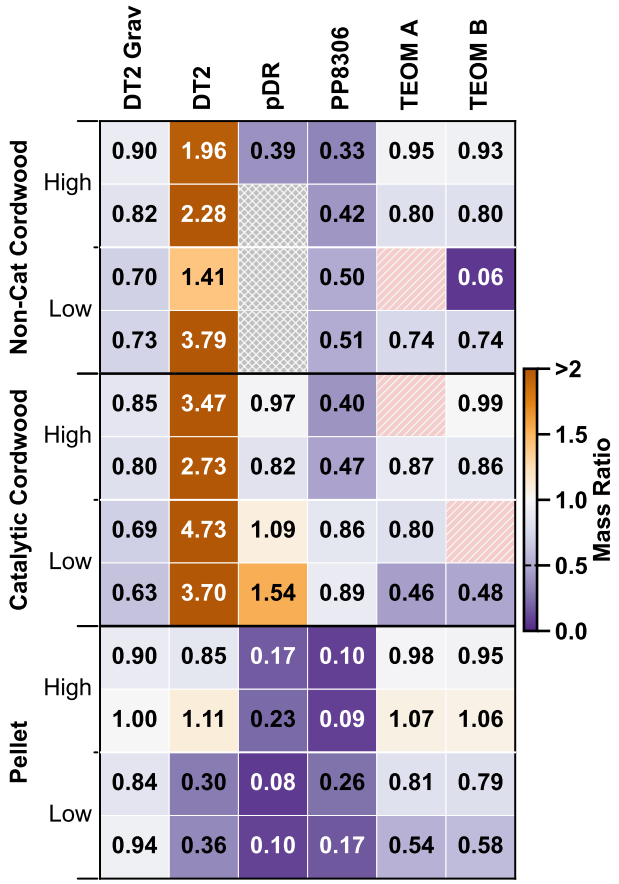


Figure 3: Mass ratio of each uncorrected real-time instrument to the gravimetric filter reference for each heater type and operating phase. Each row within an operating phase represents an individual test run (two replicate tests were conducted per phase). Ratios greater than 1.0 indicate overestimation (orange) relative to the reference, while ratios less than 1.0 indicate underestimation (purple). Hatched cells indicate phases where the instrument reported a negative cumulative mass. pDR data was not collected for three of the non-catalytic cordwood tests due to user error. The TEOM channel A reported negative mass for two cordwood tests while channel B reported negative mass for one cordwood test.

Several possible explanations for the DT2's underestimation were considered. The ratio pattern across burn phases and heater types suggests that aerosol composition may be contributing to the DT2's underestimation. Researchers have shown that PM from pellet combustion is predominantly solid inorganic material, consisting mainly of potassium and sulfate salts, while PM from cordwood combustion is dominated by organic matter and elemental carbon [17, 19, 26]. The lower ratios observed for heaters producing primarily organic PM suggest that evaporative loss of semi-volatile organics due to filter heating within the DT2 may be a contributing factor. Specifically, we hypothesize that internal temperatures within the DT2 enclosure may have increased over the course of a sampling day, resulting in elevated filter temperatures and greater evaporative losses during low-burn phases, which were always conducted later in the day. Although filter temperature inside the DT2 cassette was not monitored, post-test investigation revealed that temperatures near the DT2 filter cassette reached 28–29 °C during operation, consistently 5–7 °C above the reference filter and ambient. The cassette temperature continued to rise over the first hour of pump operation, with peak temperatures coinciding with the period in which low-burn sampling would typically begin (see Figure S8). While internal heating of the DT2 enclosure represents a source of negative bias, this is a known and tolerable limitation of in-situ optical measurements, where the ability to deploy a compact, battery-powered instrument in the field outweighs the cost of a modest systematic underestimation. This thermal bias may be partially reduced by using the DT2 with an external pump; however, temperatures within the enclosure were observed to increase even with the internal pump off, suggesting that pump heat is not the sole contributor to filter heating and that an external pump configuration may only partially mitigate this effect (see Figure S8).

Real-Time Instruments. The performance of each real-time instrument varied widely across heater types and operating phases, with no single instrument performing consistently well.

The DT2 exhibited a distinct pattern of overestimation for both cordwood heaters and near-unity agreement for the pellet heater during high-burn, followed by severe underestimation during pellet low-burn. Several potential explanations were considered. The calibration aerosol density (2.6 g/cm^3) substantially exceeds the effective density of wood smoke aerosol (approximately 1.1–1.6 g/cm^3 depending on fuel type), which would be expected to produce overestimation by approximately a factor of two if all else were equal. This is broadly consistent with the overestimation observed for both cordwood heaters. The refractive index assumed during calibration (1.51) is slightly lower than that reported for wood smoke (1.56), which would tend to cause underestimation, but not sufficient to offset the density-driven overestimation. For the pellet heater, about 25–30% of total PM mass (see Figure S9) falls below the DT2's stated detection limit of 0.1 µm, which would contribute to underestimation. This may also partially explain the near-unity

agreement during pellet high-burn and reflect a coincidental cancellation of competing biases. The severe underestimation during pellet low-burn (ratios of 0.30–0.36) may reflect the particle size distribution of the aerosol. Low-burn combustion produces a lower fraction of particles larger than 300 nm, which generate a disproportionately high optical response per unit mass. With fewer of these large particles present, the DT2 signal is suppressed relative to the true gravimetric mass, resulting in significant underprediction [46, 58].

The pDR performed closest to the reference during the catalytic cordwood phases, with ratios ranging from 0.82 to 1.54, which may partly reflect the greater proportion of particles in the 300 nm–1 µm range relative to non-catalytic cordwood combustion (see Figure S9, Test 1). Particles in this size range scatter light more efficiently per unit mass than the sub-300 nm particles that dominate non-catalytic exhaust[46], potentially producing a stronger pDR response relative to collected mass. For the non-catalytic cordwood heater, the pDR underestimated total PM mass during the high-burn (mass ratio of 0.39), but it is unclear if this is representative for all non-catalytic cordwood heater tests since data from three of the four phases were lost due to a pressure disturbance caused by user error. Severe underestimation was observed during pellet heater operation, with ratios ranging from 0.08 to 0.23, consistent with the dominance of sub-100 nm particles in pellet smoke, which contribute little scattered signal relative to their mass. Although the pDR and DT2 share the same stated lower detection limit of 0.1 µm, the two instruments show opposite biases for cordwood aerosol, with the pDR underestimating and the DT2 overestimating relative to the gravimetric reference. This divergence likely reflects differences in size-dependent scattering response arising from the use of different calibration dust grades, specifically A2 fine for the pDR and A1 ultrafine for the DT2, which may be related to the wavelengths of their light sources, though a full explanation would require detailed characterization of each instrument's response across the relevant particle size range.

The PP8306 underestimated PM mass across all conditions, with ratios ranging from 0.33 to 0.89 for the cordwood heaters and 0.09 to 0.26 for the pellet heater. For both cordwood heaters, ratios were consistently higher during low-burn than high-burn phases, with the catalytic cordwood low-burn producing the highest ratios overall (0.86 and 0.89). The near-unity ratios observed during catalytic cordwood low-burn phases are more difficult to interpret. Although 60% of catalytic cordwood PM mass falls below the PP8306's 300 nm detection threshold, suggesting substantial underestimation should persist, these conditions also produced a proportionally larger coarse fraction (10–20 µm), which the PP8306 can detect and which may partially offset the sub-300 nm deficit (Figure S9). This coarse-fraction effect may explain why ratios approach unity under these specific conditions, though this interpretation remains tentative. During non-catalytic cordwood operating phases, ratios ranged from 0.33 to 0.51, reflecting significant underestimation driven by the sub-300 nm particle fraction. The most severe underestimation occurred during pellet heater operation, consistent with the dominance of sub-300 nm particles in pellet smoke falling below the PP8306's optical

detection threshold. Unlike the DT2 and pDR, the PP8306 lacks an onboard gravimetric filter for site-specific calibration, relying instead on user-provided density and refractive index values to convert particle counts to mass concentration. Even with aerosol-specific optical properties derived from concurrent size-resolved measurements, the instrument substantially underestimated PM mass across most conditions, suggesting its mass conversion approach has fundamental limitations for wood smoke aerosol that cannot be resolved through optical property inputs alone.

The TEOM reported integrated mass concentrations that were closest to the reference filter, but reported non-quantitative results for 2 of the 16 tests for Channel A and 3 of the 16 tests for Channel B. For all but one test, at least one channel provided valid measurements when the other channel reported erroneous results. The TEOM performed especially well during pellet heater high-burn phases where both channels produced ratios close to unity (TEOMA: 0.98 and 1.07; TEOMB: 0.95 and 1.06). This closer agreement is expected given that the TEOM measures mass directly by monitoring changes in the resonant frequency of a tapered element and is therefore not subject to the optical size threshold that limits the three optical instruments. Performance degraded during cordwood combustion, where semi-volatile losses become more influential relative to the total mass accumulated on the tapered element. Three phases produced anomalous negative cumulative mass values (Table 2), a known artifact of the tapered-element measurement principle arising from semi-volatile absorption and desorption or mechanical shedding [4, 22, 39, 42, 54], and are excluded from the mass ratio comparison. The near-zero TEOMB ratio during the first non-catalytic cordwood low-burn (0.06) likely reflects near-detection-limit conditions rather than a true instrument bias, as the reference mass for that phase was exceptionally low (see Table 2). When both channels reported values, they generally produced similar ratios to one another; however, ratios remained variable and generally below unity, consistent with known tapered-element measurement artifacts during cordwood combustion.

Although cordwood fuel moisture (9.3–10.5% dry-basis) was below standard certification ranges (19–25% dry-basis), these results likely represent a best-case scenario for semi-volatile measurement challenges due to lower condensable organic fractions. Testing with higher-moisture fuel would likely exacerbate TEOM mass loss and optical filter volatilization, further reinforcing the instrument limitations identified in this study.

3.2. Response to Transient PM Events

To evaluate each instrument's ability to capture transient PM events, time-resolved PM mass concentrations from each instrument were compared against the size-resolved shape reference measurements across all heater types and operating phases. Instruments were generally scaled using phase-specific gravimetric correction factors (Table S8). However, for a few test phases, negative or undefined correction factors precluded standard scaling. In these instances, raw unscaled TEOM data were plotted to preserve authentic

mass-loss dynamics, while Sintrol data were omitted because PM concentrations fell below the instrument's measurement limit, yielding an undefined gravimetric calibration factor.

Figures 4 and 5 show the high-burn and low-burn phases, respectively. Data are shown as 10-second averages to align the sampling rates of the optical instruments with those of the TEOM. Figure 6 summarizes the Pearson correlation coefficient (r) between each instrument and the reference for each test and phase, providing a quantitative complement to the temporal traces. Because Pearson r is scale-invariant, it evaluates real-time tracking performance independently of gravimetric scaling. Parity plots and Bland–Altman plots for each instrument are provided in the Supplementary Data (SD) (Section S-2.8). Because candidate instruments and the size-resolved reference were generally normalized to the 47 mm gravimetric filter mass for each burn phase, the mean bias in the Bland–Altman analysis is mathematically constrained near zero by design. Consequently, the Bland–Altman limits of agreement and variance evaluate real-time tracking dynamics and temporal scatter rather than absolute calibration offset.

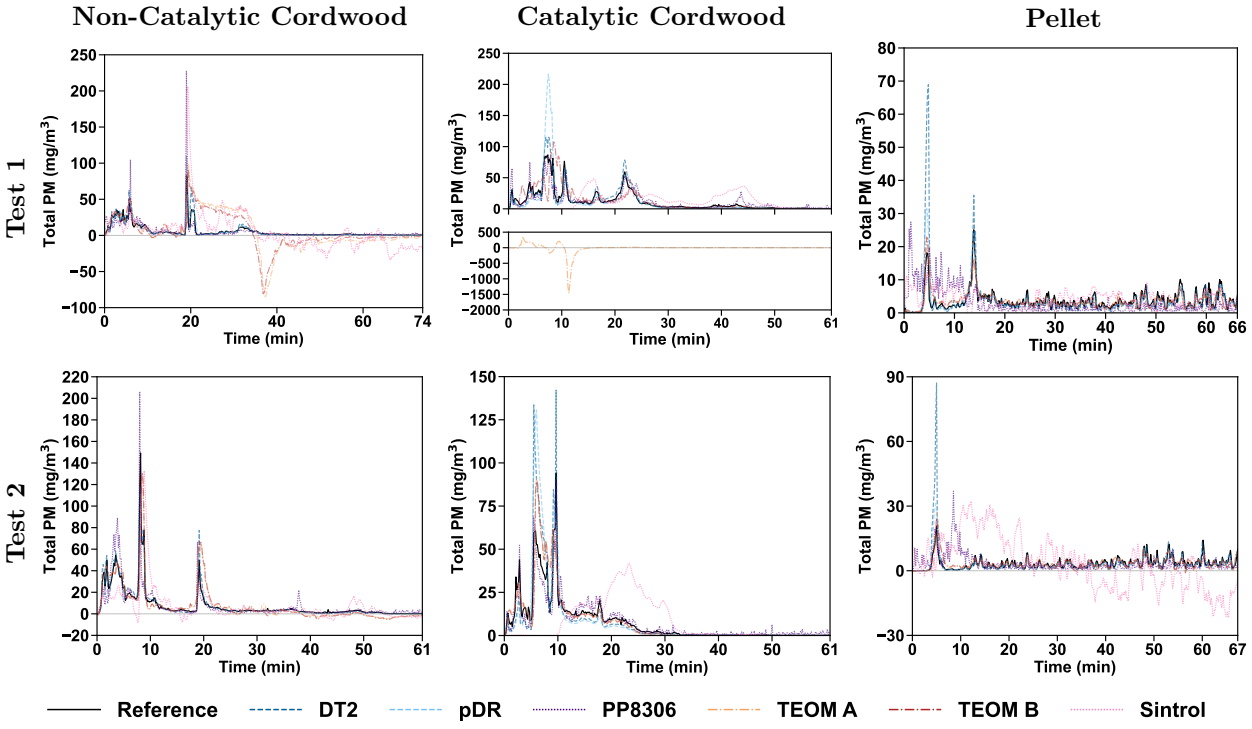


Figure 4: PM mass during high-burn phase for three heater types (columns) and two replicate tests (rows). The black solid line is the size-resolved shape reference. Continuous instruments are scaled using phase-specific gravimetric correction factors (Table S8), except for TEOM A during the Catalytic Cordwood High-1 test phase, where raw unscaled data are presented to preserve authentic mass-loss dynamics resulting from net negative mass measurements.

The DT2 and pDR consistently follow the general shape of the reference signal across all heater types and phases, capturing the emission events but not always the magnitudes. This temporal agreement is reflected in their high r values, with the DT2 returning $r \geq 0.87$ across all non-catalytic and catalytic cordwood

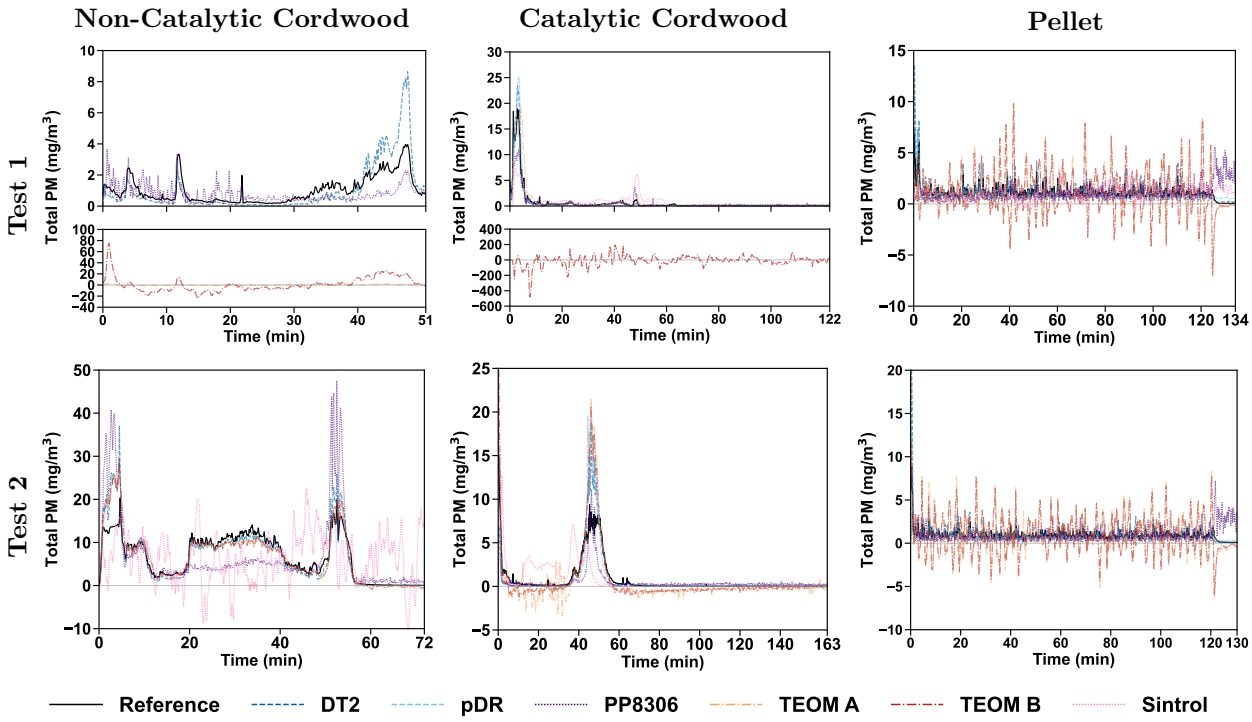


Figure 5: PM mass during low-burn phase for three heater types (columns) and two replicate tests (rows). The black solid line is the size-resolved shape reference. Continuous instruments are scaled using phase-specific gravimetric correction factors (Table S8). Raw unscaled data are presented to preserve authentic mass-loss dynamics resulting from net negative mass measurements for TEOM A during Cordwood Low-1 and TEOM B during Catalytic Cordwood Low-1. Additionally, Sintrol data are omitted during Cordwood Low-1 and Pellet Low-2 because PM concentrations fell below the instrument's measurement limit, yielding an undefined gravimetric calibration factor. Note that the automatic air control for the second low-burn test for the non-catalytic cordwood heater was engaged late, leading to higher particulate matter generation than the first test.

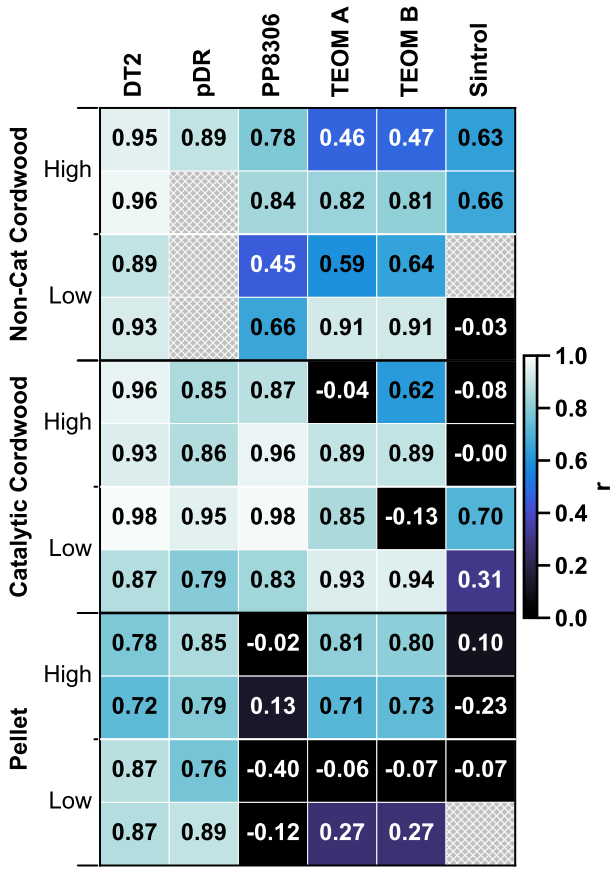


Figure 6: Pearson correlation coefficients (r) comparing real-time instruments to the size-resolved shape reference across heater types and operating conditions. pDR data was not collected for three of the non-catalytic cordwood tests due to user error.

tests, and the pDR returning $r \geq 0.79$. During the largest transient events, both instruments tend to over-predict relative to the reference. In the second catalytic cordwood high-burn (Figure 4, bottom-center), the DT2 and pDR report gravimetrically adjusted concentrations at the peak approaching 130 mg/m^3 while the reference peaks near 70 mg/m^3, yet both instruments faithfully reproduce the shape and timing of the event. Bland–Altman plots (Figure S13) confirm this proportional bias increases with concentration. The first pellet high-burn (Figure 4, top-right) shows a similar pattern, with the DT2 and pDR reporting startup peaks roughly two to three times those of the reference, while still tracking the subsequent decay. Outside of these high-concentration transients, the optical instruments agree closely with the reference, suggesting that the over-prediction reflects the optical response to elevated loadings or shifts in particle optical properties (Figures S12 and S14).

The PP8306 tracks the general trend of the reference well for all catalytic cordwood heater tests (r=0.83–0.98) and the high-burn test for the non-catalytic cordwood heater (r=0.78 and 0.84). The temporal tracking degraded during the low-burn phases of the non-catalytic cordwood heater, with r values of 0.45 and 0.66. This indicates that the instrument struggled to follow concentration fluctuations at lower emission levels. Performance of the gravimetrically-adjusted PP8306 is poor across all pellet tests where the instrument does not meaningfully track reference trends (r=−-0.40–0.13). This is likely due to almost all of the PM mass consisting of particles with diameters smaller than the instrument's detection limit (300 nm), as discussed in Section 3.1.

The TEOM exhibits inconsistent temporal agreement that varies by test and phase. While most test phases reflect gravimetrically scaled concentrations, raw unscaled data are presented for TEOM channel A during Non-Catalytic Cordwood low-burn test 1 and Catalytic Cordwood high-burn test 1, and for TEOM channel B during Catalytic Cordwood low-burn test 1 to preserve authentic mass-loss dynamics. During the second non-catalytic cordwood high-burn and both catalytic cordwood low-burns, both channels return $r \geq 0.89$, indicating tight tracking of reference trends during moderate, sustained emission events. However, temporal agreement can deteriorate following high-concentration transients, where the instrument signal drops sharply and can become strongly negative. The first non-catalytic cordwood high-burn (Figure 4, top-left), for example, returns r values of 0.46 and 0.47 for both channels, reflecting the TEOM's failure to follow the reference during the initial high-emission period and the TEOM's subsequent oscillation through negative values. The most extreme measurement and disagreement between channels that should be nominally equivalent occurred during the first catalytic cordwood high-burn, where TEOM channel A shows concentrations as high as 1500 mg/m^3 shortly after the startup peak (Figure 4, top-center), resulting in an r of 0.04 for that channel. These negative concentrations are also reflected in the cumulative mass, where both channels overshoot the gravimetric reference during the startup and then steadily lose mass for the

remainder of the phase (Figure S10, top-left). During the pellet heater low-burn phases, the TEOM signal frequently oscillates around zero and reports negative values, with both channels returning negative r values for the first low burn.

The two channels also diverge from one another, as shown in the first non-catalytic cordwood low-burn. With both channels nominally equivalent, this divergence is unexpected, particularly as the instrument reported no errors or data quality flags during the experiment. The most extreme divergence occurs during the first catalytic cordwood test (both high- and low-burn phases), which were conducted consecutively on the same day. Subsequent review of the logged flow rate data revealed that flow rates on both channels dropped by approximately 50% roughly 10 minutes after heater startup during the first catalytic cordwood high-burn, coinciding with filter loading reaching ∼98%. According to the EPA-recommended standard operating procedure, this flow rate excursion would constitute a failed measurement and invalidate the affected data [45], yet no real-time indication of degraded data quality was provided by the instrument during sampling. Flow rates returned to the nominal 1 LPM after both filters were changed at the end of the high-burn phase. However, divergence between the channels persisted during the low-burn, with channel B demonstrating poor temporal tracking ($r = 0.13$) and channel A tracking well ($r = 0.85$). These results indicate that the flow excursion alone does not fully explain the observed artifacts, pointing instead to the tapered-element measurement principle itself, where particle losses arise from mechanical shedding of the oscillating filter or absorption and desorption of semi-volatile compounds on and off the collection filter [4, 22, 39, 42, 54]. The artifacts observed here may be a fundamental consequence of applying the TEOM outside its design regime, as the instrument was intended for slowly varying ambient aerosol rather than the rapid, high concentration swings produced by a wood heater [61].

The Sintrol tracks moderately with the reference during the cordwood high-burns, with r values of 0.63 and 0.66 for the two non-catalytic cordwood high-burns. During the catalytic cordwood high-burns, the Sintrol consistently shows a false increase in signal after engaging the catalyst around 10 minutes (Figure 4, center column), yielding r values of -0.08 and -0.00. The combined effect of under-reporting during startup and the false post-catalyst peak produces the bow-tie pattern visible in the Bland–Altman plots (Figure S23). The increase in signal did not correspond to temperature or humidity changes in the dilution tunnel. Triboelectric instruments like the Sintrol are known to be sensitive to particle charge and composition, both of which may have shifted following catalyst engagement. During the low-burn phases, the Sintrol r values are near zero or negative across all heater types, indicating no meaningful temporal tracking. For the pellet tests the Sintrol performs poorly across all phases, with r values ranging from -0.28 to 0.10, indicating the concentrations may be below its measurement limit. Across all test phases, the Sintrol logged data as a 50-second average against 10-second reference data. This time-averaging mismatch may dampen emission spikes

and contribute to lower overall correlation (r). Sintrol data were omitted during Non-Catalytic Cordwood Low-1 and Pellet Low-2 because PM concentrations fell below the instrument's measurement limit, yielding an undefined gravimetric calibration factor.

3.3. Implications for Field Deployment

Although none of the instruments were investigated during in-situ measurement, several outcomes from this laboratory study can help inform instrument selection and operational expectations for field deployment of real-time PM monitors in test facilities and in homes. The instrument's suitability for field use depends not only on measurement agreement but also on practical considerations such as setup complexity, consumable requirements, portability, and the quality and timeliness of error reporting. Table 3 summarizes each instrument's operating principle, specifications, key operational observations, and tracking performance obtained in this study, and the discussion below elaborates on each of these considerations.

Measurement Agreement and Gravimetric Correction. The suitability of each instrument depends heavily on the intended application, as no single instrument performed well across all heater types, operating conditions, and measurement goals. For applications requiring accurate integrated mass, the gravimetric mass ratios reported without correction reveal that no optical instrument reliably reproduced the reference mass across all conditions, with ratios ranging from 0.08 to 3.79 depending on instrument and phase. Gravimetric correction reduced this variability but required co-located filter samples collected under the same conditions, and correction factors were not stable across aerosol types or operating conditions. The optical instruments require a co-located gravimetric filter to provide accurate mass measurements. In field settings where filter changes are logistically difficult or where continuous unattended operation is required, this dependency on consumable filters may limit the practicality of optical instruments for quantitative mass measurement. The TEOM avoids this limitation as a direct mass instrument, but the data quality issues observed in this study are concerning, and present additional practical barriers to field deployment. For applications requiring only real-time trend tracking, such as identifying emission events or comparing relative performance across burn conditions, the gravimetrically-corrected DT2 and pDR showed the most consistent temporal agreement with the reference across heater types, with r values of 0.87–0.98 and 0.79–0.96 respectively. The Sintrol showed the weakest temporal tracking overall ($r \leq 0.66$), and the TEOM showed the widest variability ($r =$ 0.04–0.94), driven largely by the filter artifacts described in Section 3.2.

Cost and Consumables. Beyond measurement agreement, the instruments also differ in cost and consumable requirements. The PP8306 is one of the least expensive instruments evaluated (tied with the Sintrol at $5,000) and additionally reports particle number concentration ($\#\ 1/\mathrm{cm}^3$) along with calculated size-resolved particle

mass ($PM_{0.5}$, PM_1, $PM_{2.5}$, PM_{10}, and total PM). The TEOM is the most expensive ($25,000–$40,000) and is the only instrument providing a direct mass measurement, a method widely used in regulatory ambient air monitoring. It should be noted that Thermo Scientific announced they plan to discontinue the 1405-D TEOM in June 2026. The DT2 and pDR offer an integrated 37 mm filter ($2.20 per filter) with no data-collection delay following a filter change. The TEOM operates with two Pallflex TX40 13 mm filters (∼$40 each), which must be replaced at minimum before each test phase and potentially mid-phase during high-PM events, which could result in data loss. After each filter change, the TEOM requires 5 to 10 minutes before resuming data collection. The Sintrol contains no consumable parts but requires application-specific calibration.

Portability, Setup, and Error Reporting. The DT2, pDR, and PP8306 are best suited for field measurements owing to their smaller size and weight, battery-power option, and onboard data storage. The TEOM is substantially larger and heavier than the optical instruments (roughly 24–72 times the volume and 7–18 times the weight), and requires AC power. While most instruments required less than 15 minutes to set up with no specialized training, the TEOM setup required an expert user approximately one hour, with post-test data validation and processing requiring additional expertise.

The DT2 and PP8306 display error messages on screen when a fault is detected, while the pDR freezes the display on the last recorded value without an explicit alert. The TEOM reports status and error codes on its front panel, but the indicators do not include real-time warnings of degraded data quality during sampling. For example, the flow rate excursion observed during the first catalytic cordwood high-burn (Figure 4) was only identifiable through post-hoc review of logged flow data by a trained expert. Since real-time indication of measurement failure is not available to the operator, data that would constitute a failed measurement under EPA-recommended procedures may not be identified until after the test is complete [45]. Less experienced users may therefore face an even greater risk of undetected measurement failures. The Sintrol provides only a rudimentary LED status indicator, with two states relevant to field use: Normal Operation (solid green) and FAULT (blinking red), where FAULT indicates no valid signal is being generated. Normal Operation does not differentiate between reliable and unreliable signals, meaning conditions such as concentrations below the detection limit or interference from catalyst engagement will not trigger any alert, as was observed during this study.

Table 3: Overview of particulate instruments evaluated.

	DustTrak II 8530	**pDR-1500**	**Particles Plus 8306**	**1405-D TEOM[a]**	**Sintrol S203**
Operational notes	Robust; setup <15 min; briefly exceeded max conc. at startup	Robust; setup <15 min; no data for 3 tests due to sampling line disturbance	Compact; PM mass and size; setup <15 min; requires additional dilution beyond dilution tunnel	Setup >1 hr; observed filter mass-loss and sustained negative cumulative mass	Best for direct stack measurement; setup <15 min; requires application specific calibration
Pearson Correlation (r)[b]	0.87–0.98	0.79–0.96	−0.33–0.96	−0.59–0.94	−0.41–0.70
Gravimetric mass ratio[c]	0.63–1.00 (filter) 0.30–3.79 (optical)	0.08–1.54	0.09–1.14	0.06–1.07	N/A
Operating principle	Optical	Optical	Optical	Mass (TEOM)	Triboelectric
Conc. range (mg/m^3)	0.001–400	0.001–400	0.00001–20	0–1000	0.01–>1000
Form factor	13.5×21.6×22.4 cm; 1.6–2.5 kg; battery	18.1×14.3×8.4 cm; 1.2 kg; battery	13.0×10.8×31.1 cm; 1.0 kg; battery	43.2×48.3×75 cm; 18 kg; AC only	65.6×16.8×17.5 cm; 1.5 kg; AC only
Data acquisition[d]	1 s native; 60,000 samples internal; streaming	1 s native; 500,000 samples internal; streaming	1 s native; 45,000 samples internal; streaming	10 s native; 500,000 samples internal; streaming	Not stated; PC log only; streaming
Approx. cost (USD)[e]	$8,600	$10,000	$5,000	$25,000–40,000	$5,000
Gravimetric correction	Required; integrated 37 mm filter	Required; integrated 37 mm filter	Required; external filter	Not required (direct mass)	N/A (TSP only)
Per-test consumables[f]	$2.20/filter; no resumption delay	$2.20/filter; no resumption delay	External filter; no resumption delay	∼$80/test (2 filters); 5–10 min resumption after change	None
Zero calibration	Yes (user)	Yes (user)	Zero check only	Not available	Zero check only

[a] Thermo Scientific will discontinue the 1405-D TEOM on June 30, 2026.
[b] Pearson correlation coefficient (r) calculated from 10-s averaged data. TEOM r represents the best performing channel per phase.
[c] Ratio of instrument-integrated mass to the gravimetric filter reference across all tests and phases, where 1.0 indicates perfect agreement. Values are reported without gravimetric correction. TEOM range represents the best performing channel per phase.
[d] Native measurement interval; internal storage capacity; streaming capability.
[e] Estimated 2026 USD; see Table S11 for full breakdown including consumables.
[f] Approximate cost of consumable filters per test phase and time required for instrument to resume data collection after a filter change.

4. Conclusions

The purpose of this study was to evaluate five continuous PM instruments against gravimetric filter references and size-resolved reference concentrations across three residential wood heater types and two operating phases, with the goal of informing instrument selection for laboratory test facilities and potential field deployment. Overall, no single instrument performed well across all heater types, operating conditions, and measurement goals, and instrument selection necessarily involves tradeoffs between mass accuracy, temporal resolution, and practical deployability.

The results demonstrate that neither optical nor direct-mass measurement principles are well-matched to the full range of conditions produced by residential wood heaters. Optical instruments are fundamentally constrained by the mismatch between their calibration aerosols and wood smoke aerosol. For some heaters and operating conditions, a substantial fraction of particle mass may fall below the instruments' size detection limit, rendering it effectively invisible to optical monitors. Condition-specific gravimetric correction factors were also not stable across fuel types or operating conditions, suggesting they cannot be assumed to transfer reliably between fuel or heater types. The TEOM, despite providing direct mass measurement without gravimetric correction, performed poorly during cordwood combustion, where the rapid, high-concentration transients produced conditions outside its design regime and introduced a risk of undetected measurement failure. For applications requiring real-time trend tracking rather than absolute mass, the DT2 and pDR outperformed both the TEOM and the PP8306. This suggests that more complex instruments do not necessarily perform better for wood heater PM monitoring.

Several instruments show strong promise for specific heaters and operating conditions; however, further research is needed to evaluate instrument performance across a broader range of stove types, operating conditions, wood species, and moisture contents. Concurrent black carbon measurements in future studies would help clarify how shifts in aerosol composition drive instrument-specific biases across fuel types and burn conditions. Opacity sensors represent a further avenue for investigation, as they may reduce reliance on dilution tunnels; however, they would still require calibration to relate opacity to PM mass. Future studies could also collect filter samples at higher frequency during low-burn or transition phases to investigate time-varying particle density shifts.

CRediT authorship contribution statement

VHR: Conceptualization, Formal Analysis, Funding Acquisition, Investigation, Methodology, Project Administration, Supervision, Validation, Visualization, Writing – Original Draft, Writing – Review & Editing. **BCS**: Conceptualization, Funding Acquisition, Validation, Writing – Original Draft, Writing – Review

& Editing. **RT**: Formal Analysis, Investigation, Methodology, Validation, Visualization, Writing – Original Draft, Writing – Review & Editing. **SSC**: Investigation, Validation, Visualization, Writing – Original Draft, Writing – Review & Editing. **DAB**: Investigation, Validation, Visualization, Writing – Original Draft, Writing – Review & Editing. **WD**: Conceptualization, Investigation, Validation, Writing – Review & Editing. **EA**: Conceptualization, Funding Acquisition, Supervision, Validation, Writing – Review & Editing. **JC**: Conceptualization, Funding Acquisition, Supervision, Validation, Writing – Review & Editing.

Declaration of Generative AI and AI-Assisted Technologies in the Writing Process

During the preparation of this work, the author(s) used the CBorg AI platform provided by the IT Division at the Lawrence Berkeley National Laboratory (Supported by the Director, Office of Science, Office of Basic Energy Sciences, of the U.S. Department of Energy under Contract No. DE-AC02-05CH11231) to improve language clarity, readability, and to assist with the structural proofreading of the manuscript text. After using this tool, the authors reviewed and edited the content as needed and take full responsibility for the final content of the publication.

Acknowledgments

The work described in this study was conducted at Lawrence Berkeley National Laboratory and supported by the U.S. Department of Energy Bioenergy Technologies Office under Contract No. DE-AC02-05CH11231.

This research used the CBorg AI platform and resources provided by the IT Division at the Lawrence Berkeley National Laboratory (Supported by the Director, Office of Science, Office of Basic Energy Sciences, of the U.S. Department of Energy under Contract No. DE-AC02-05CH11231). CBorg was used to assist in engineering and data-handling tasks during the research process. This included generating scripts for logging data from new instruments, integrating those scripts into our existing data acquisition infrastructure, refining the cosmetic features of figures, and debug code. All code and results were reviewed, tested, and verified by the authors. The authors also acknowledge the use of Google's NotebookLM to assist in reviewing literature identified by the authors. The tool was utilized strictly to query published literature databases created by the authors and cross-reference our data-driven arguments against existing academic precedents.

The authors gratefully acknowledge Mark Shmorhun for project oversight, support, and technical review. We also thank our industry partners for their valuable contributions: Chris Neufeld and Corie Podschelne for providing test equipment and technical guidance.

References

[1] Alfano, B., Barretta, L., Del Giudice, A., De Vito, S., Di Francia, G., Esposito, E., Formisano, F., Massera, E., Miglietta, M.L., Polichetti, T., . A review of low-cost particulate matter sensors from the developers' perspectives. Sensors 20, 6819. URL: https://www.mdpi.com/1424-8220/20/23/6819, doi:10.3390/s20236819.

[2] Allen, G., Morin, B., Ahmadi, M., Rector, L., a. Online measurement of pm from residential wood heaters in a dilution tunnel. Journal of the Air & Waste Management Association 72, 662–678. URL: https://www.tandfonline.com/doi/full/10.1080/10962247.2022.2049927, doi:10.1080/10962247.2022.2049927.

[3] Allen, G., Rector, L., Butcher, T., Trojanowski, R., 2017. Evaluation of alternative filter media for particulate matter emission testing of residential wood heating devices. Journal of the Air & Waste Management Association 67, 1055–1060. URL: https://doi.org/10.1080/10962247.2017.1349011, doi:10.1080/10962247.2017.1349011.

[4] Allen, G., Sioutas, C., Koutrakis, P., Reiss, R., Lurmann, F.W., Roberts, P.T., b. Evaluation of the TEOM® method for measurement of ambient particulate mass in urban areas. Journal of the Air & Waste Management Association 47, 682–689. URL: https://www.tandfonline.com/doi/full/10.1080/10473289.1997.10463923, doi:10.1080/10473289.1997.10463923.

[5] ASTM International, a. ASTM E2515-11 Test Method for Determination of Particulate Matter Emissions Collected by a Dilution Tunnel. Technical Report E2515-11. ASTM International. URL: http://www.astm.org/cgi-bin/resolver.cgi?E2515-11R17, doi:10.1520/E2515-11R17.

[6] ASTM International, b. ASTM E2618-13 Standard Test Method for Measurement of Particulate Emissions and Heating Efficiency of Solid Fuel-Fired Hydronic Heating Appliances. Technical Report E2618-13. ASTM International. URL: https://www.astm.org/e2618-13r19.html.

[7] ASTM International, c. ASTM E2779-10 Test Method for Determining Particulate Matter Emissions from Pellet Heaters. Technical Report E2779-10. ASTM International. URL: http://www.astm.org/cgi-bin/resolver.cgi?E2779-10R17, doi:10.1520/E2779-10R17.

[8] ASTM International, d. ASTM E2780-10 Test Method for Determining Particulate Matter Emissions from Wood Heaters. Technical Report E2780-10. ASTM International. URL: http://www.astm.org/cgi-bin/resolver.cgi?E2780-10R17, doi:10.1520/E2780-10R17.

[9] ASTM International, e. ASTM E3053-18e2 Standard Test Method for Determining Particulate Matter Emissions from Wood Heaters Using Cordwood Test Fuel. Technical Report E3053-18e2. ASTM International. URL: http://www.astm.org/cgi-bin/resolver.cgi?E3053-17, doi:10.1520/E3053-17.

[10] ASTM International, f. Test Methods for Direct Moisture Content Measurement of Wood and Wood-Based Materials. Technical Report. ASTM International. URL: http://www.astm.org/cgi-bin/resolver.cgi?D4442-20, doi:10.1520/D4442-20.

[11] Bioenergy International, 2022. DOE selects six projects to advance US wood heaters. Technical Report. Bioenergy International. Published: April 14, 2022. Accessed: May 22, 2026.

[12] Bland, J.M., Altman, D.G., 2007. Agreement Between Methods of Measurement with Multiple Observations Per Individual. Journal of Biopharmaceutical Statistics 17, 571–582. URL: https://www.tandfonline.com/doi/full/10.1080/10543400701329422, doi:10.1080/10543400701329422.

[13] Blaze King Industries, 2025. Sirocco SC30.2 Solid Fuel Wood Catalytic Stove Operation & Installation Manual. Valley Comfort Systems Inc. URL: https://www.blazeking.com/wp-content/uploads/2025/02/180-SC30.2-v3.01.pdf.

[14] Boman, C., Pettersson, E., Westerholm, R., Boström, D., Nordin, A., . Stove performance and emission characteristics in residential wood log and pellet combustion, part 1: Pellet stoves. Energy & Fuels 25, 307–314. URL: https://pubs.acs.org/doi/10.1021/ef100774x, doi:10.1021/ef100774x.

[15] Brandelet, B., Rose, C., Landreau, J., Druette, L., Rogaume, Y., . Toward a cleaner domestic wood heating by the optimization of firewood stoves? Journal of Cleaner Production 325, 129338. URL: https://linkinghub.elsevier.com/retrieve/pii/S095965262103523X, doi:10.1016/j.jclepro.2021.129338.

[16] Butcher, T., Trojanowski, R., 2020. Effect of thermal storage on the emissions and efficiency performance of a wood pellet-fired residential boiler. ACS Omega 5. URL: https://www.osti.gov/biblio/1668663, doi:10.1021/acsomega.0c03080.

[17] Bäfver, L.S., Leckner, B., Tullin, C., Berntsen, M., 2011. Particle emissions from pellets stoves and modern and old-type wood stoves. Biomass and Bioenergy 35, 3648–3655. doi:https://doi.org/10.1016/j.biombioe.2011.05.027.

[18] Caubel, J., Trojanowski, R., Butcher, T., Rapp, V., 2023. A review of regulatory standard test methods for residential wood heaters and recommendations for their advancement. Renewable and

Sustainable Energy Reviews 184, 113501. URL: https://linkinghub.elsevier.com/retrieve/pii/S1364032123003581, doi:10.1016/j.rser.2023.113501.

[19] Chandrasekaran, S.R., Laing, J.R., Holsen, T.M., Raja, S., Hopke, P.K., . Emission characterization and efficiency measurements of high-efficiency wood boilers. Energy & Fuels 25, 5015–5021. URL: https://pubs.acs.org/doi/10.1021/ef2012563, doi:10.1021/ef2012563.

[20] Charron, A., . Quantitative interpretation of divergence between PM10 and PM2.5 mass measurement by TEOM and gravimetric (partisol) instruments. Atmospheric Environment 38, 415–423. URL: https://linkinghub.elsevier.com/retrieve/pii/S1352231003008616, doi:10.1016/j.atmosenv.2003.09.072.

[21] CSA Group, . CSA B415.1:22 Performance testing of solid-biofuel-burning heating appliances. Technical Report CSA B415.1:22. CSA Group. URL: https://www.csagroup.org/store/product/2701332/.

[22] DeCarlo, P.F., Slowik, J.G., Worsnop, D.R., Davidovits, P., Jimenez, J.L., . Particle morphology and density characterization by combined mobility and aerodynamic diameter measurements. part 1: Theory. Aerosol Science and Technology 38, 1185–1205. URL: http://www.tandfonline.com/doi/abs/10.1080/027868290903907, doi:10.1080/027868290903907.

[23] Delmhorst, 2011. Delmhorst BD2100 User Manual 510INS-0006 Rev. 01/11. URL: https://www.emlab.com/m/store/Delmhorst%20BD2100%20User%20Manual.pdf.

[24] Despotović, v.V., 2013. Some Experiences in the Exploitation of Triboelectric Sensors for Measuring Concentration of Particulate Matter on Thermal Power Plants. URL: https://www.viser.edu.rs/uploads/2020/03/TES-2_Z.Despotovic_INFOTEH_2013.pdf. presented at INFOTEH-JAHORINA 2013, Paper Ref: TES-2.

[25] European Committee for Standardization, . EN 16510-1:2022 Residential solid fuel burning appliances. Part 1: General requirements and test methods. Technical Report EN 16510-1:2022. European Committee for Standardization. URL: https://www.en-standard.eu/bs-en-16510-1-2022-residential-solid-fuel-burning-appliances-general-requirements-and-test-methods,

[26] Fachinger, F., Drewnick, F., Gieré, R., Borrmann, S., . How the user can influence particulate emissions from residential wood and pellet stoves: Emission factors for different fuels and burning conditions. Atmospheric Environment 158, 216–226. URL: https://linkinghub.elsevier.com/retrieve/pii/S1352231017301590, doi:10.1016/j.atmosenv.2017.03.027.

[27] Giavarina, D., 2015. Understanding Bland Altman analysis. Biochemia Medica 25, 141–151. URL: http://www.biochemia-medica.com/en/journal/25/2/10.11613/BM.2015.015, doi:10.11613/BM.2015.015.

[28] Hagan, D.H., Kroll, J.H., 2020. Assessing the accuracy of low-cost optical particle sensors using a physics-based approach. Atmospheric Measurement Techniques 13, 6343–6355. URL: https://amt.copernicus.org/articles/13/6343/2020/, doi:10.5194/amt-13-6343-2020.

[29] Hand, J.L., Kreidenweis, S.M., . A new method for retrieving particle refractive index and effective density from aerosol size distribution data. Aerosol Science and Technology 36, 1012–1026. URL: http://www.tandfonline.com/doi/abs/10.1080/02786820290092276, doi:10.1080/02786820290092276.

[30] Hauck, H., Berner, A., Gomiscek, B., Stopper, S., Puxbaum, H., Kundi, M., Preining, O., . On the equivalence of gravimetric PM data with TEOM and beta-attenuation measurements. Journal of Aerosol Science 35, 1135–1149. URL: https://linkinghub.elsevier.com/retrieve/pii/S0021850204000667, doi:10.1016/j.jaerosci.2004.04.004.

[31] International Organization for Standardization, 2018. Determination of particle size distribution — Light scattering airborne particle counter for clean spaces. Standard ISO 21501-4:2018. International Organization for Standardization. Geneva, Switzerland. URL: iso.org.

[32] Kingham, S., Durand, M., Aberkane, T., Harrison, J., Gaines Wilson, J., Epton, M., . Winter comparison of TEOM, MiniVol and DustTrak PM10 monitors in a woodsmoke environment. Atmospheric Environment 40, 338–347. URL: https://linkinghub.elsevier.com/retrieve/pii/S1352231005008885, doi:10.1016/j.atmosenv.2005.09.042.

[33] Kinsey, J.S., Kariher, P.H., Dong, Y., . Evaluation of methods for the physical characterization of the fine particle emissions from two residential wood combustion appliances. Atmospheric Environment 43, 4959–4967. URL: https://linkinghub.elsevier.com/retrieve/pii/S1352231009005895, doi:10.1016/j.atmosenv.2009.07.008.

[34] Kortekand, M., de Vries, J., van Berkel, P., de Bruyn, S., 2022. Health-related social costs of air pollution due to residential heating and cooking in the EU27 and UK. Report 22.190144.027. CE Delft. URL: https://cedelft.eu/publications/health-related-social-costs-of-air-pollution-due-to-residential-heating-and-cooking-in-the-eu27-an

[35] Kortelainen, M., Jokiniemi, J., Tiitta, P., Tissari, J., Lamberg, H., Leskinen, J., Grigonyte-Lopez Rodriguez, J., Koponen, H., Antikainen, S., Nuutinen, I., Zimmermann, R., Sippula, O., . Time-

resolved chemical composition of small-scale batch combustion emissions from various wood species. Fuel 233, 224–236. URL: https://linkinghub.elsevier.com/retrieve/pii/S0016236118311049, doi:10.1016/j.fuel.2018.06.056.

[36] Krieger, U.K., Rupp, S., Hausammann, E., Peter, T., 2007. Simultaneous measurements of pm10 and pm1 using a single teom. Aerosol Science and Technology 41, 975–980. doi:10.1080/02786820701639715.

[37] Kulkarni, P., Baron, P.A., Willeke, K., 2011. Aerosol Measurement: Principles, Techniques, and Applications. 3rd ed ed., John Wiley & Sons, Incorporated, Hoboken.

[38] Levin, E.J.T., McMeeking, G.R., Carrico, C.M., Mack, L.E., Kreidenweis, S.M., Wold, C.E., Moosmüller, H., Arnott, W.P., Hao, W.M., Collett, J.L., Malm, W.C., 2010. Biomass burning smoke aerosol properties measured during fire laboratory at missoula experiments (FLAME). Journal of Geophysical Research: Atmospheres 115, 2009JD013601. URL: https://agupubs.onlinelibrary.wiley.com/doi/10.1029/2009JD013601, doi:10.1029/2009JD013601.

[39] Li, Q.F., Wang-Li, L., Liu, Z., Heber, A.J., . Field evaluation of particulate matter measurements using tapered element oscillating microbalance in a layer house. Journal of the Air & Waste Management Association 62, 322–335. URL: https://www.tandfonline.com/doi/full/10.1080/10473289.2011.650316, doi:10.1080/10473289.2011.650316.

[40] Lin, L.I.K., 1989. A Concordance Correlation Coefficient to Evaluate Reproducibility. Biometrics 45, 255. URL: https://www.jstor.org/stable/2532051?origin=crossref, doi:10.2307/2532051.

[41] Martin Bland, J., Altman, D., 1986. Statistical Methods for Assessing Agreement Between Two Methods of Clinical Measurement. The Lancet 327, 307–310. URL: https://linkinghub.elsevier.com/retrieve/pii/S0140673686908378, doi:10.1016/S0140-6736(86)90837-8.

[42] Mignacca, D., Stubbs, K., . Effects of equilibration temperature on PM_{10} concentrations from the TEOM method in the lower fraser valley. Journal of the Air & Waste Management Association 49, 1250–1254. URL: https://www.tandfonline.com/doi/full/10.1080/10473289.1999.10463914, doi:10.1080/10473289.1999.10463914.

[43] Misiulia, D.I., Kuz'min, V.V., Markov, V.A., . Developing an untwisting device for cyclones and estimating its parameters. Theoretical Foundations of Chemical Engineering 47, 274–283. URL: https://link.springer.com/10.1134/S004057951303007X, doi:10.1134/S004057951303007X.

[44] Moosmüller, H., Arnott, W.P., Rogers, C.F., Bowen, J.L., Gillies, J.A., Pierson, W.R., Collins, J.F., Durbin, T.D., Norbeck, J.M., 2001. Time resolved characterization of diesel particulate emissions. 1. instruments for particle mass measurements. Environmental Science & Technology 35, 781–787. doi:10.1021/es0013935.

[45] New York State Energy Research and Development Authority, 2025. NYSERDA Standard Operation Procedures for use of a Thermo Scientific 1405-D TEOM in a dilution tunnel with wood-fired stoves, hydronic heaters, and furnaces with calculations for grams PM emitted for EPA Independent Assessment Project. Standard Operating Procedure EPA-HQ-OAR-2016-0130-0076. New York State Energy Research and Development Authority (NYSERDA). URL: https://www.regulations.gov/document/EPA-HQ-OAR-2016-0130-0076. submitted to EPA docket EPA-HQ-OAR-2016-0130. Accessed 2026-05-14.

[46] Ouimette, J.R., Malm, W.C., Schichtel, B.A., Sheridan, P.J., Andrews, E., Ogren, J.A., Arnott, W.P., . Evaluating the PurpleAir monitor as an aerosol light scattering instrument. Atmospheric Measurement Techniques 15, 655–676. URL: https://amt.copernicus.org/articles/15/655/2022/, doi:10.5194/amt-15-655-2022.

[47] Particles Plus, Inc., 2019. 8000 Series Handheld Particle Counters User's Manual. Particles Plus, Inc.. Stoughton, MA, USA. URL: https://www.particlesplus.com. copyright 2019 by Particles Plus, Inc.

[48] Quadra-Fire, 2024. Quadra-Fire 4300 Installation Manual - 7037-801G. URL: https://downloads.hearthnhome.com/installManuals/43M_ACC_C_43ST_ACC_C_WOOD_STOVE_INSTALLATION_7037_801.pdf.

[49] Rapp, V.H., Caubel, J.J., Wilson, D.L., Gadgil, A.J., 2016. Reducing Ultrafine Particle Emissions Using Air Injection in Wood-Burning Cookstoves. Environmental Science & Technology 50, 8368–8374. URL: https://pubs.acs.org/doi/10.1021/acs.est.6b01333, doi:10.1021/acs.est.6b01333.

[50] Rapp, V.H., Chen, S.S., Anacleto-Black, D., Putaansuu, N., . Evaluation of a Smoke Opacity Sensor for Improving Residential Wood Heater Combustion. Technical Report LBNL-2001749. LBNL. URL: https://escholarship.org/uc/item/4250w1jg, doi:10.20357/B79G77.

[51] Regency Fireplace Products, . Greenfire GF55 & GFI55 Freestanding and Fireplace Insert Pellet Heater Owner's Manual. URL: https://assets.regency-fire.com/getattachment/19d62113-e7fb-4ff4-89d0-8da02cad2e82/GF55-GFI55-Owners-Manual-(2).aspx.

[52] Roessler, D.M., Faxvog, F.R., 1979. Opacity of black smoke: calculated variation with particle size and refractive index. Applied Optics 18, 1399. URL: https://opg.optica.org/abstract.cfm?URI=ao-18-9-1399, doi:10.1364/AO.18.001399.

[53] SAE International, 2018. J1667-201802 Snap acceleration smoke test procedure for heavy-duty diesel powered vehicles. Technical Report. SAE International. URL: https://www.sae.org/standards/j1667_201802-snap-acceleration-smoke-test-procedure-heavy-duty-diesel-powered-vehicles, doi:10.4271/J1667_201802.

[54] Salvador, C.M., Chou, C.C.K., . Analysis of semi-volatile materials (SVM) in fine particulate matter. Atmospheric Environment 95, 288–295. URL: https://linkinghub.elsevier.com/retrieve/pii/S1352231014004920, doi:10.1016/j.atmosenv.2014.06.046.

[55] Schön, C., Hartmann, H., 2018. Status of PM emission measurement methods and new developments. Technical Report. IEA Bioenergy. Task 32.

[56] Schwab, J.J., Spicer, J., Demerjian, K.L., Ambs, J.L., Felton, H.D., . Long-term field characterization of tapered element oscillating microbalance and modified tapered element oscillating microbalance samplers in urban and rural new york state locations. Journal of the Air & Waste Management Association 54, 1264–1280. URL: https://www.tandfonline.com/doi/full/10.1080/10473289.2004.10470998, doi:10.1080/10473289.2004.10470998.

[57] Seabold, S., Perktold, J., 2010. Statsmodels: Econometric and Statistical Modeling with Python, in: SciPy Proceedings, Austin, Texas. pp. 92–96. URL: https://doi.curvenote.com/10.25080/Majora-92bf1922-011, doi:10.25080/Majora-92bf1922-011.

[58] Singer, B.C., Delp, W.W., . Response of consumer and research grade indoor air quality monitors to residential sources of fine particles. Indoor Air 28, 624–639. URL: https://onlinelibrary.wiley.com/doi/10.1111/ina.12463, doi:10.1111/ina.12463.

[59] Sintrol Oy, 2023. S200 Series Dust Monitors User Manual: Models S201 and S203. Sintrol Oy. Helsinki, Finland. URL: https://sintrol.com. revision 6, Publication date: 2023-06-07.

[60] Standards Australia, Standards New Zealand, 2014. AS/NZS 4013:2014 Domestic solid fuel burning appliances—Method for determination of flue gas emission. Standard. Standards Australia and Standards New Zealand. Sydney, NSW and Wellington, NZ.

[61] Sullivan, B., Allawatt, G., Emery, A., Means, P., Kramlich, J., Posner, J., . Time-resolved particulate emissions monitoring of cookstove biomass combustion using a tapered element oscillating microbalance. Combustion Science and Technology 189, 923–936. URL: https://www.tandfonline.com/doi/full/10.1080/00102202.2016.1253564, doi:10.1080/00102202.2016.1253564.

[62] Thermo Fisher Scientific, . TEOM 1405-D Dichotomous Ambient Particulate Monitor Operator's Manual. Environmental Instruments Division. URL: http://tools.thermofisher.com/content/sfs/manuals/EPM-TEOM1405D-Manual.pdf.

[63] Thermo Fisher Scientific, 2022. MIE pDR-1500 Active Personal Particulate Monitor Instruction Manual. Air Quality Instruments. Franklin, MA, USA. URL: https://www.thermofisher.com. part Number 105983-00.

[64] Thielke, J.F., Pilat, M.J., 1978. Plume opacity related to particle mass concentration and size distribution. Atmospheric Environment (1967) 12, 2439–2447. URL: https://linkinghub.elsevier.com/retrieve/pii/0004698178902883, doi:10.1016/0004-6981(78)90288-3.

[65] Trojanowski, R., 2025. A Comparison of Novel Woodstove Catalytic Combustors to Improve Low Temperature Light off and Catalyst Stability at High Temperatures and Corrosive Environments, Including Stability of Catalytic Combustors used in Coastal Environments. Technical Report. Brookhaven National Laboratory (BNL), Upton, NY (United States); Applied Ceramics Inc., Atlanta, GA (United States). URL: https://www.osti.gov/biblio/2572567, doi:10.2172/2572567.

[66] Trojanowski, R., Fthenakis, V., 2019. Nanoparticle emissions from residential wood combustion: A critical literature review, characterization, and recommendations. Renewable and Sustainable Energy Reviews 103, 515–528. URL: https://linkinghub.elsevier.com/retrieve/pii/S1364032119300012, doi:10.1016/j.rser.2019.01.007.

[67] TSI Incorporated, 2012. DustTrak II Aerosol Monitor Theory of Operation. Application Note EXPMN-001, Rev. C. TSI Incorporated. Shoreview, MN, USA. Printed in U.S.A.

[68] TSI Incorporated, 2023. Model 8530/8530EP/8532 DustTrak II Aerosol Monitor Operation and Service Manual. TSI Incorporated. Shoreview, MN, USA. URL: https://www.tsi.com. p/N 6001893, Revision W.

[69] U.S. Department of Energy, 2025. U.S. Department of Energy Selects Three Projects to Advance Wood Heater Innovation to Access Affordable, Renewable Energy. Technical Report. U.S. Department of

Energy. Office of Energy Efficiency and Renewable Energy, Bioenergy Technologies Office. Published: January 16, 2025. Accessed: May 22, 2026.

[70] U.S. Energy Information Administration, 2023. Table CE7.2: Household Wood Consumption in the United States—Totals and Averages, 2020. 2020 Residential Energy Consumption Survey (RECS). U.S. Department of Energy, Office of Energy Consumption and Efficiency Statistics. URL: https://www.eia.gov/consumption/residential/data/2020/index.php?view=consumption.

[71] U.S. Environmental Protection Agency, . ALT-140 Approval of Integrated Duty Cycle Test Method (IDC) for Subpart AAA Wood Heater Compliance Testing. Technical Report ALT-140. U.S. Environmental Protection Agency. URL: https://www.epa.gov/system/files/documents/2021-07/atm_14_2.pdf.

[72] U.S. Environmental Protection Agency, 2020. Method 5 –Determination of Particulate Matter Emissions from Stationary Sources. Federal Test Method 40 CFR Part 60, Appendix A-3. U.S. EPA Air Emission Measurement Center (EMC). URL: https://www.epa.gov/emc/method-5-particulate-matter-pm. promulgated December 7, 2020.

[73] U.S. Environmental Protection Agency, 2026. EPA-certified wood heater database. https://www.epa.gov/compliance/epa-certified-wood-heater-database. Accessed: 2026-09-27.

[74] US EPA, 2019. Method 28R—Certification and Auditing of Wood Heaters. United States Environmental Protection Agency. Washington, DC. 40 CFR Part 60, Appendix A-8.

[75] Wang, K., Nakao, S., Thimmaiah, D., Hopke, P.K., a. Emissions from in-use residential wood pellet boilers and potential emissions savings using thermal storage. Science of The Total Environment 676, 564–576. URL: https://linkinghub.elsevier.com/retrieve/pii/S0048969719318601, doi:10.1016/j.scitotenv.2019.04.325.

[76] Wang, X., Robbins, C., Hoekman, S.K., Chow, J.C., Watson, J.G., Schuetzle, D., b. Dilution sampling and analysis of particulate matter in biomass-derived syngas. Frontiers of Environmental Science & Engineering in China 5, 320–330. URL: http://link.springer.com/10.1007/s11783-011-0347-x, doi:10.1007/s11783-011-0347-x.

[77] Wang, X., Watson, J.G., Chow, J.C., Gronstal, S., Kohl, S.D., c. An efficient multipollutant system for measuring real-world emissions from stationary and mobile sources. Aerosol and Air Quality Research 12, 145–160. URL: https://aaqr.org/articles/aaqr-11-11-oa-0187, doi:10.4209/aaqr.2011.11.0187.

[78] von der Weiden, S.L., Drewnick, F., Borrmann, S., 2009. Particle loss calculator – a new software tool for the calculation of particle losses in transport systems. Atmospheric Measurement Techniques 2, 479–494. doi:10.5194/amt-2-479-2009.

Supplementary Data for
Evaluating real-time particulate matter instruments against gravimetric and size-resolved references to advance residential wood heater development

Vi H. Rapp, Brett C. Singer, Rebecca Trojanowski, Sharon S. Chen, Dylan Anacleto-Black, William W. Delp, Eric Adair, and John Crouch

S-1. Supporting Methods

S-1.1. Secondary Dilution System

Table S1: Summary of dilution tunnel and secondary dilution system flow metrics across test phases.

Phase	Dilution Tunnel Flow Rate	Secondary Dilution Sample Flow Rate	Secondary Dilution Air Flow Rate	Secondary Dilution Factor (phase-average)
Cordwood High	500 SCFM	1.2 SLPM	43.2 SLPM	38
Cordwood Low	500 SCFM	3.0–5.2 SLPM	10.2–36.0 SLPM	3–13
Cat. Cordwood High	500 SCFM	1.3 SLPM	43.2 SLPM	36
Cat. Cordwood Low	500 SCFM	1.2–5.1 SLPM	10.4–16.9 SLPM	3–15
Pellet High	300 SCFM	2.9 SLPM	42 SLPM	15
Pellet Low	300 SCFM	3.2 SLPM	12.4 SLPM	5

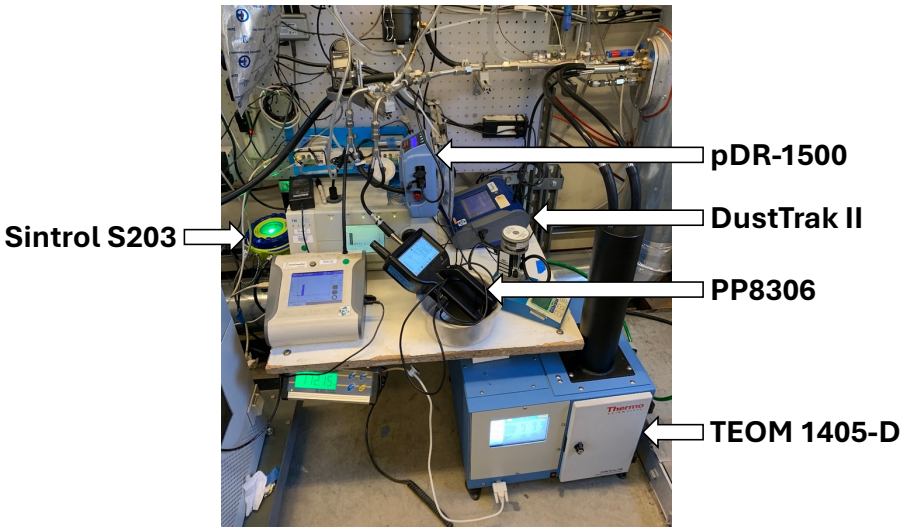


Figure S1: Image of sampling lines from dilution tunnel, secondary dilution system, and particle instruments.

S-1.2. Chimney Specifications

Chimney dimensions and total heights for each heater are summarized in Table S2. Each chimney comprised single-wall stove pipe topped with 1-inch (2.54 cm) double-wall insulated pipe, with a stove-pipe connector at the base where required. The pellet heater's rear-facing exhaust port required a single-wall tee connector to route the chimney upward; the physical heater itself was 0.87 m (34.125 in.) tall, though this dimension does not contribute to the total stack height since the exhaust exits from the rear.

Table S2: Heights of heaters and stack components. Total height is measured from the top of the scale to the top of the chimney.

	Cordwood	Catalytic-Cordwood	Pellet
Chimney Diameter (internal)	15.24 cm (6 in.)	15.24 cm (6 in.)	10.16 cm (4 in.)
Scale to Stack Base[a]	0.81 m (31.875 in.)	0.77 m (30.5 in.)	0.51 m (20.25 in.)
Stove-pipe Connector	7.62 cm (3 in.)	—	12.7 cm (5 in.)[b]
Single-wall Stove Pipe	1.63 m (64 in.)	1.63 m (64 in.)	1.68 m (66 in.)
Insulated Chimney	2.11 m (83 in.)	2.11 m (83 in.)	2.03 m (80 in.)
Total Height	4.62 m (181.875 in.)	4.51 m (177.5 in.)	4.35 m (171.25 in.)

[a] For the cordwood and catalytic-cordwood heaters, this is the heater height, since the stack rises from the top of the heater. For the pellet heater, this is the distance from the scale to the center of the rear-facing exhaust port.

[b] Single-wall tee connector used to route the rear-facing exhaust upward.

S-1.3. Heater Operating Procedures

Figures S2 through S7 show the fuel loads and air control settings for each heater and operating phase. A detailed description of the high-burn and low-burn procedures are provided in Tables S3 and S4.

Table S3: High-burn operating protocol for the three heater types. All high-burn phases begin with a cold (room-temperature) firebox, cleaned of ash from previous burns. Times in the Events column are minutes from ignition (cordwood, cat-cordwood) or from power-on (pellet).

Heater	Initial Fuel Load	Initial Settings	Events (time: action)	Duration (min)
Cordwood	100 g paper knots, 1.0 kg kindling, 1.2–1.4 kg small logs; door open	Burn Rate Air Control = 5; Automatic Combustion Control (ACC) lever = "HI"	0–1: lighting; 3–5: (optional) shut door; 5–8: load 2 small logs (1.6–1.9 kg); 6–9: shut door; 19–20: load 2–4 large logs (2.4–5.1 kg); 20–21: shut door	60–74
Cat-Cordwood	50 g paper knots, 0.75 kg kindling; door open	Catalytic combustor bypassed; thermostat knob = 100%	0–1: lighting; 2–4: load 3 small logs (1.4–1.5 kg); 5–6: shut door; 8–9: load 2 large logs (2.2–2.4 kg); 9–10: shut door; 10–11: engage catalytic combustor	60
Pellet	Burn pot clean; hopper filled with Douglas fir pellets	Feed Trim = 4; Combustion Air Trim = 2; Heat Level = 5	0–3: burn-pot fills with pellets; 3–4: 300 W ignitor activates; 4–5: flames established; 10–12: room air fan initiates, automated startup complete	65

Table S4: Low-burn operating protocol for the three heater types. The cordwood heaters begin from a robust bed of hot coals with a fresh fuel load and the door closed; the pellet heater begins from active operation. Each cordwood phase ends when less than 1.0 kg of fuel remains in the firebox. Times in the Events column are minutes from reload (cordwood, cat-cordwood) or from heat-level selection (pellet).

Heater	Initial Fuel Load	Initial Settings	Events (time: action)	Duration (min)
Cordwood	2 large logs (1.2 kg) freshly loaded	Burn Rate Air Control = 1; ACC lever pulled to front; ACC air control timer activated	0–5: choked combustion air [a]	50–72
Cat-Cordwood	3 large logs (2.8–2.9 kg) freshly loaded	Catalytic combustor engaged; thermostat knob = 100%	5: reduce thermostat knob from 100% to 85%; 10: reduce thermostat knob from 85% to 70%	122–163
Pellet	Hopper filled with Douglas fir pellets	Feed Trim = 4; Combustion Air Trim = 2; Heat Level = 2	120–125: heater turned off, pellet burn-out begins	130–135

[a] This only occurred for Test 2 and was an operator error.



Figure S2: Images of the cordwood heater high-burn phase paper knots (a), kindling (b), small fuel logs (c), large fuel logs (d), air-control settings (e), firebox before lighting (f), and firebox after all fuel is loaded (g).

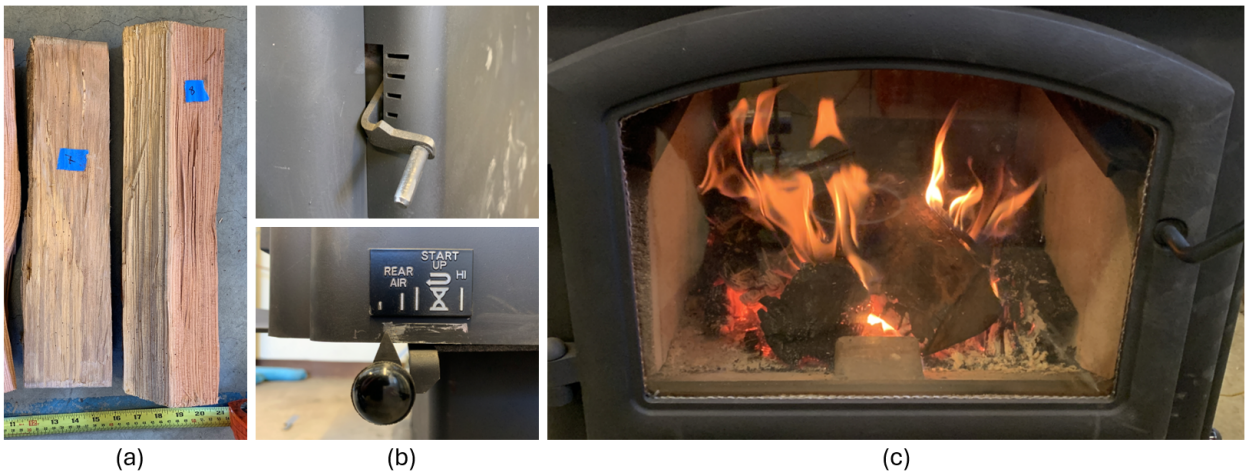


Figure S3: Images of the cordwood heater low-burn phase fuel logs (a), air-control settings (b), and firebox after loading the fuel (c).



Figure S4: Images of the catalytic-cordwood heater high-burn phase paper knots (a), kindling (b), small fuel logs (c), large fuel logs (d), air-control settings (e), firebox before lighting (f), and firebox after all fuel is loaded (g).

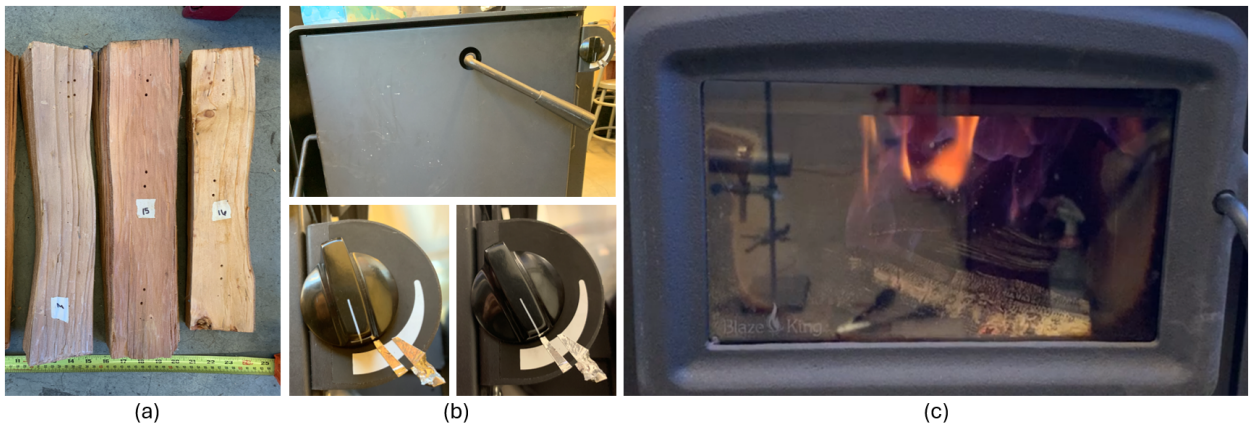


Figure S5: Images of the catalytic-cordwood heater low-burn phase fuel logs (a), air-control settings (b), and firebox after loading the fuel (c).



Figure S6: Images of the pellet heater high-burn phase thermostat settings (a), and firebox (b).



Figure S7: Images of the pellet heater low-burn phase thermostat settings (a), and firebox (b)

S-1.4. Fuel Properties

All heaters were fueled with Douglas Fir seasoned cordwood sourced locally in 2023 or pellets purchased in 2020. Cordwood fuel moisture content (dry-basis) was assessed daily using a pin-type handheld moisture meter with 5/16-inch uninsulated electrodes [23]. Average moisture content of logs used per phase is shown in Table S5. Pellet fuel moisture content was assessed weekly following Method B of the oven-drying procedure described in ASTM D4442 [10]. Fuel charges were weighed on a 10 kg balance (0.1 g readability), and heaters were installed on a 200 kg platform scale (0.05 kg readability, 1 Hz logging) to monitor fuel mass burned throughout each test. Fuel properties, including ultimate analysis and heating values, are reported in Tables S6 and S7.

Table S5: Fuel moisture content (dry basis, %) by heater and phase.

Phase	**Test**	**Catalytic-Cordwood (%)**	**Cordwood (%)**	**Pellet (%)**
High	1	9.29	9.86	5.89
	2	10.00	9.87	5.89
Low	1	9.92	10.48	5.89
	2	10.19	9.52	5.89

Table S6: Fuel analysis results from Douglas fir cordwood sample.

Moisture, Total D3173 (wt%)	Ash, Total D3174		Heating Value E711		Carbon D5373	H_2 D5373	N_2 D5373	O_2, Calc.
	As Rec. (wt%)	Moist. Free (wt%)	As Rec. (BTU/lb)	Moist. Free (BTU/lb)	Moist. Free (wt%)	Moist. Free (wt%)	Moist. Free (wt%)	Moist. Free (wt%)
10.15	0.01	0.01	8,187	9,112	49.52	6.3	<0.1	44.1

Table S7: Fuel analysis results from pellet sample.

Parameter	Method	Units	Moisture Free	As Received
Ash	ASTM D1102	wt.%	0.16	0.16
Volatile Matter	ASTM D3175	wt.%	84.12	82.27
Fixed Carbon (by difference)	ASTM D3172	wt.%	15.72	15.38
Sulfur	ASTM D4239	wt.%	0.013	0.012
SO_2	Calculated	lb/mmbtu	—	0.029
Net Cal. Value (Const. Pressure)	ISO 1928	GJ/tonne	18.48	18.02
Gross Cal. Value (Const. Vol.)	ASTM E711	Btu/lb	8,735	8,543
Carbon	ASTM D5373	wt.%	47.33	46.29
Hydrogen*	ASTM D5373	wt.%	8.51	8.32
Nitrogen*	ASTM D5373	wt.%	<0.20	<0.20
Oxygen*	ASTM D3176	wt.%	>43.79	>42.83

*As-received values do not include hydrogen and oxygen in the total moisture.

S-1.5. Size-resolved Instrument Settings

The size-resolved mass reference was reconstructed from three particle size spectrometers: a TSI 3321 Aerodynamic Particle Sizer (APS), TSI 3330 Optical Particle Sizer (OPS), and TSI 3091 Fast Mobility Particle Sizer (FMPS). Settings for each instrument are as follows:

TSI Model 3091 Fast Mobility Particle Sizer (FMPS). The FMPS was left at default settings, measuring particle count and size distribution at 1 Hz for sizes ranging from 5.6 nm to 560 nm (mobility diameter). Its measurable concentration range varies from 10^2–10^7 particles/cc for the smallest particles, to 1–10^5 particles/cc for the largest particles. To preserve measurement accuracy, the electrometers were cleaned every 2 test-days.

TSI Model 3330 Optical Particle Sizer (OPS). The OPS was operated with the following user-input settings:

- Particle Density = 1.26
- Refractive index real=1.56, imaginary = 0.03, shape CF=1
- Dead Time Correction enabled

The instrument measures particle count and size distribution at 1 Hz for size ranging from 0.3 µm to 10 µm (optical diameter). It implements a light scattering technique (660 nm wavelength laser; 120 degree light collection) and has a measurable concentration range of 0–3000 particles/cc. Its native 37 mm filter cartridge enables gravimetric sampling that was not used in this study.

TSI Model 3321 Aerodynamic Particle Sizer (APS). The APS was left at default settings, measuring particle count and size distribution at 1 Hz for sizes ranging from 0.5 µm to 20 µm (aerodynamic diameter). It has a measurable concentration range of 0.001–10^4 particles/cc.

S-2. Supporting Results

S-2.1. Filter Temperature Comparison

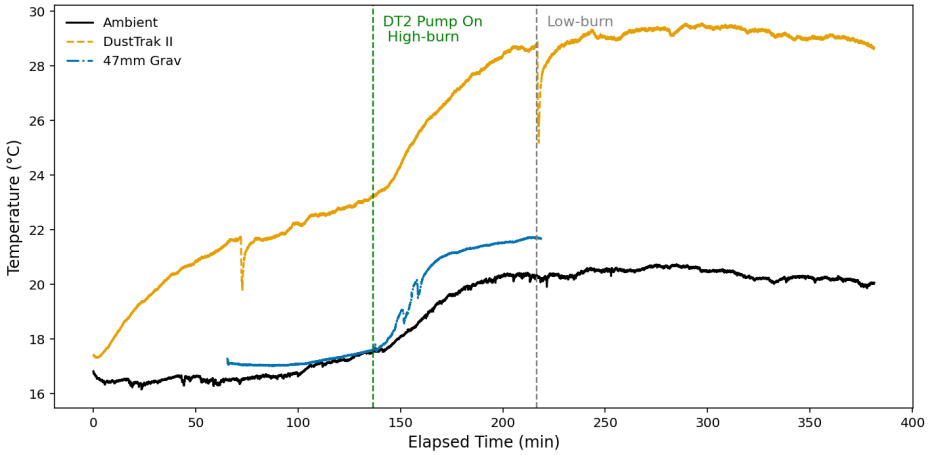


Figure S8: Temperature measurements recorded near the DustTrak II filter cassette, in the reference gravimetric filter holder (47mm Grav), and in the room (Ambient). The dashed vertical line indicates the time at which the heater was ignited, the DustTrak II pump was activated, and flow through the 47mm Grav filter was started. Temperatures near the DustTrak II filter cassette remained elevated above ambient throughout operation and continued to rise over the first hour of pump operation, approaching peak values at approximately the time low-burn sampling phases would typically begin. Ambient and 47mm Grav temperatures also increased following heater ignition as the test space warmed.

S-2.2. Instrument Correction Factors

Table S8: Gravimetric correction factors for continuous PM instruments across heater types and operating phases, defined as the ratio of gravimetric reference mass to integrated real-time mass.

Heater	Phase	DT2	pDR	PP8306	TEOM A	TEOM B	Sintrol
Non-Catalytic Cordwood	Startup 1	0.570	3.168	4.716	0.962	1.047	1.711×10^{-1}
	Startup 2	0.393	1.848	2.401	1.115	1.105	1.848×10^{-1}
	High 1	0.454	2.100	2.129	1.087	1.025	2.089×10^{-1}
	High 2	0.634	1.844	2.351	1.736	1.757	8.103×10^{-2}
	Low 1	0.709	1.311	1.585	N/A[a]	14.851	N/A[b]
	Low 2	0.264	15.837	1.974	1.343	1.354	1.810×10^{-1}
Catalytic Cordwood	High 1	0.288	1.033	2.475	N/A[a]	1.006	6.061×10^{-4}
	High 2	0.367	1.222	2.121	1.149	1.158	3.871×10^{-4}
	Low 1	0.211	0.916	1.021	1.304	N/A[a]	2.279×10^{-4}
	Low 2	0.270	0.637	0.878	2.034	1.925	2.353×10^{-4}
Pellet	High 1	1.167	5.740	8.741	1.025	1.053	7.055×10^{-2}
	High 2	0.898	4.360	11.413	0.940	0.949	1.513×10^{-1}
	Low 1	3.344	12.714	3.733	1.223	1.245	1.475×10^{-2}
	Low 2	2.801	9.590	5.740	1.821	1.700	N/A[b]

[a] Omitted due to net negative cumulative mass catch over the phase; raw unscaled concentration data is plotted in Figures 4 & 5 to avoid artificial signal inversion.

[b] Omitted because PM concentrations fell below the instrument's measurement limit, rendering gravimetric calibration physically undefined.

S-2.3. Size resolved particle distribution

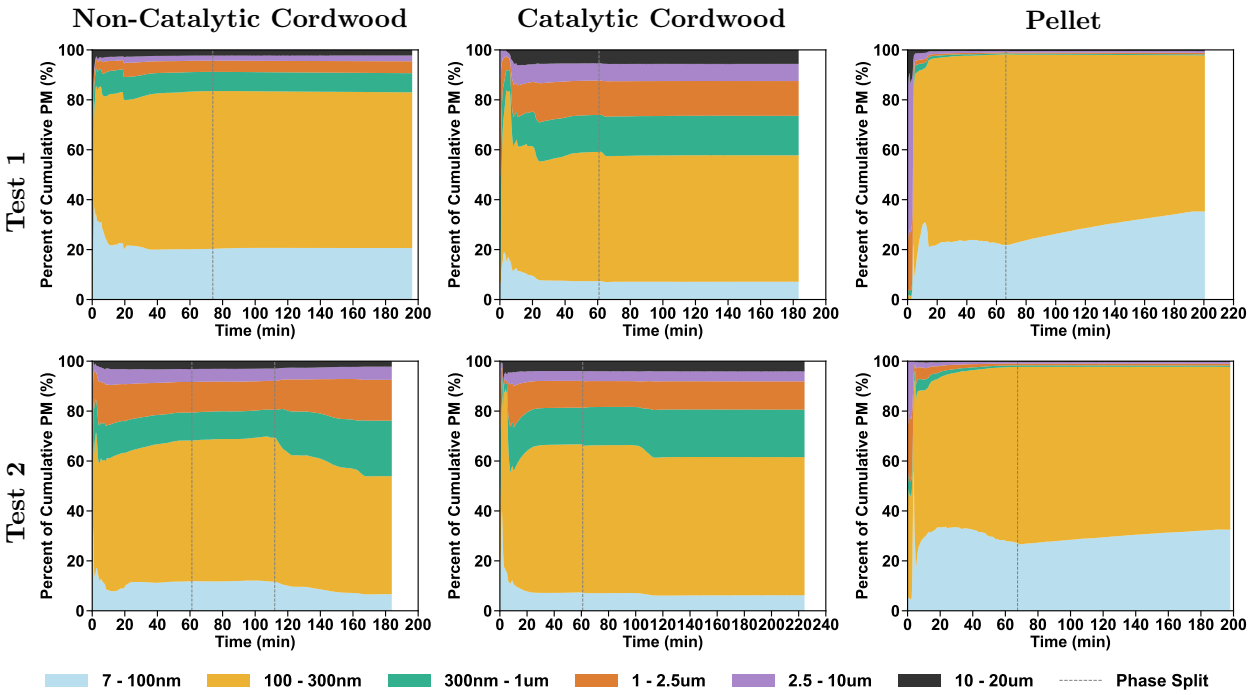


Figure S9: Stacked area plot showing the size distribution of cumulative PM mass as a function of time for the non-catalytic cordwood heater, catalytic cordwood heater, and pellet heater for each test day. The gray vertical lines separate the high-burn and low-burn phases. For the second non-catalytic cordwood test, the high-burn was followed by two low-burns. At each time step, the cumulative mass in each size bin is expressed as a fraction of the total cumulative mass collected up to that point, such that the stack sums to 100% throughout the test.

S-2.4. Calculated average particle densities

Calculated particle densities using measurements from the FMPS, APS, and OPS are shown in Table S9.

Table S9: Fuel density (g/cm^3) for each heater by test phase. Two replicate runs are shown per condition.

Phase	Run	Non-Catalytic Cordwood	Catalytic-Cordwood	Pellet
High	1	1.365	1.308	1.226
	2	1.363	1.301	1.113
Low	1	1.624	1.290	1.374
	2	1.443	1.623	1.201

S-2.5. Cumulative PM Mass

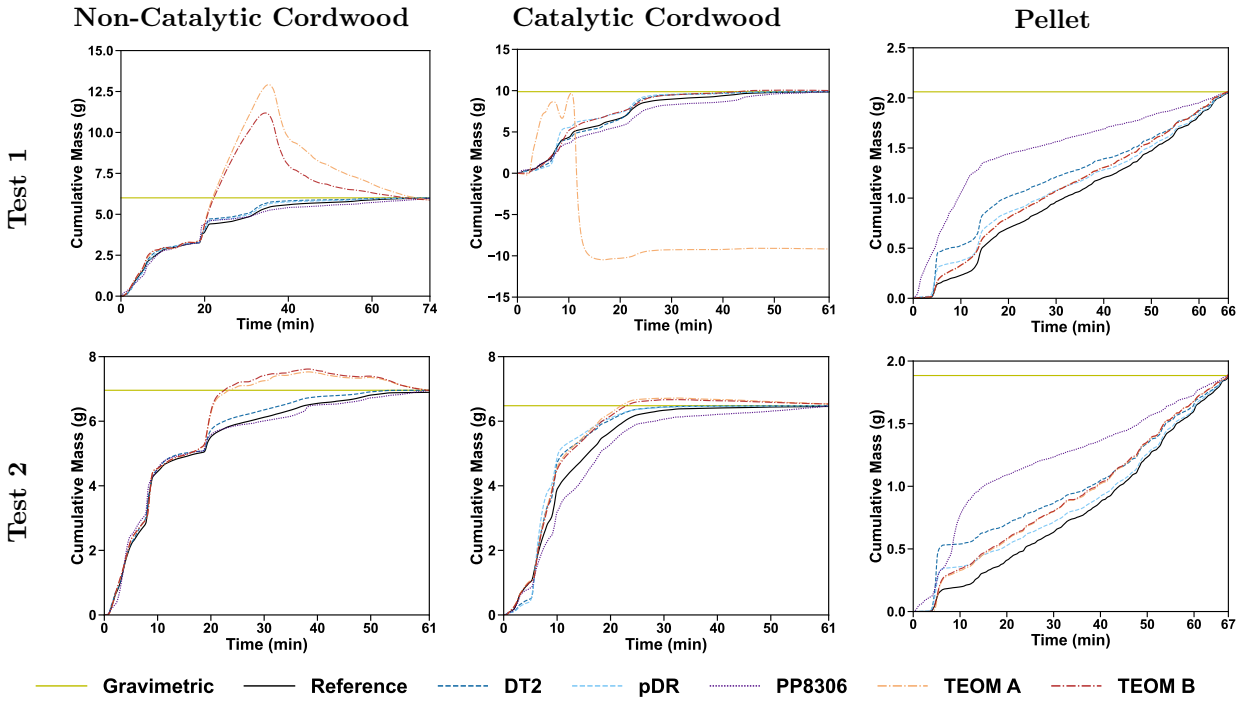


Figure S10: Cumulative PM mass during high-burn phase for three heater types (columns) and two replicate tests (rows). Yellow solid line is the gravimetric measurement reference and the black solid line is the size-resolved shape reference. Real-time instruments are scaled using phase-specific gravimetric correction factors (Table S8). For phases where net cumulative mass catch was negative, TEOM curves reflect raw unscaled data to preserve authentic mass-loss dynamics, while Sintrol curves are omitted where concentrations fell below its measurement limit..

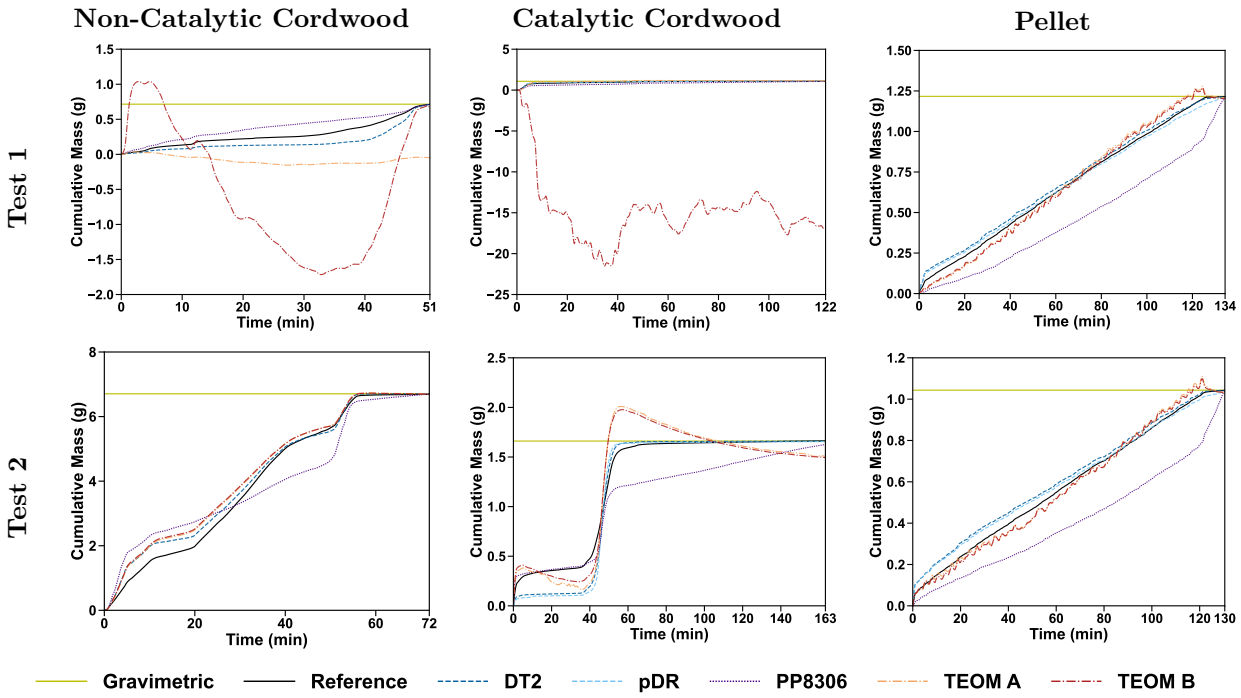


Figure S11: Cumulative PM mass during low-burn phase for three heater types (columns) and two replicate tests (rows). Yellow solid line is the gravimetric measurement reference and the black solid line is the size-resolved shape reference. Real-time instruments are scaled using phase-specific gravimetric correction factors (Table S8). For phases where net cumulative mass catch was negative, TEOM curves reflect raw unscaled data to preserve authentic mass-loss dynamics, while Sintrol curves are omitted where concentrations fell below its measurement limit.

S-2.6. Modified Combustion Efficiency

Modified Combustion Efficiency (MCE) was calculated from dilution tunnel CO_2 and CO measurements at 10-second logging intervals. An ambient CO_2 monitor was used to track background concentrations ($CO_{2,\text{ambient}}$). Phase-integrated MCE was calculated as:

$$\text{MCE}_{\text{integrated}} = \frac{\sum_t \Delta\text{CO}_2(t)}{\sum_t \Delta\text{CO}_2(t) + \sum_t \Delta\text{CO}(t)} \tag{S1}$$

where $\Delta\text{CO}_2(t) = \max(0, \text{CO}_2(t) - \text{CO}_{2,\text{ambient}})$ and $\Delta\text{CO}(t) = \text{CO}(t)$ (assuming zero ambient CO).

Table S10: Modified Combustion Efficiency (MCE) across heater types and operating phases.

Heater	Phase	MCE
Non-Catalytic Cordwood	High 1	0.980
	High 2	0.976
	Low 1	0.954
	Low 2	0.901
Catalytic Cordwood	High 1	0.971
	High 2	0.989
	Low 1	0.970
	Low 2	0.981
Pellet	High 1	0.997
	High 2	0.997
	Low 1	0.996
	Low 2	0.997

S-2.7. Detailed Description of Particle Instruments Evaluated

Table S11: In depth overview of particulate instruments evaluated.

	DustTrak II 8530	**pDR-1500**	**Particles Plus 8306**	**1405-D TEOM[a]**	**Sintrol S203**
Operating principle	Optical	Optical	Optical	Mass (TEOM)	Triboelectric
Reports PM0.3	No	No	Calculated	No	No
Reports PM0.5	No	No	Calculated	No	No
Reports PM1	With impactor	With cyclone	Calculated	No	No
Reports PM2.5	With impactor	With cyclone	Calculated	Direct	No
Reports PM4	With impactor	With cyclone	No	No	No
Reports PM5	No	No	Calculated	No	No
Reports PM10	With impactor	With cyclone	Calculated	Direct	No
Reports Total PM	Yes	Yes	Calculated	Yes	No
Native reporting[a]	Total PM	Total PM	PM0.3, PM0.5, PM1, PM2.5, PM5, PM10	PM2.5, PM10, Total PM	TSP
Reports multiple PM bins simultaneously	No	No	Yes; PM0.3, PM0.5, PM1, PM2.5, PM5, PM10	Yes; PM2.5, PM10, Total PM	N/A
Reports PM size distribution	No	No	Yes	No	No
Particle size range	0.1–10 µm	0.1–10 µm	0.3–25 µm (calculated)	None stated–10 µm	0.3 µm–TSP (200 µm optimal max.)
Particle conc. range[b]	N/A	N/A	530–1060 particles/cm^3	N/A	N/A
Conc. range[c]	0.001–400 mg/m^3	0.001–400 mg/m^3	0.00001–20 mg/m^3	0–1000 mg/m^3	0.01–>1000 mg/m^3
Resolution	0.001 mg/m^3	0.001 mg/m^3	None stated	0.0001 mg/m^3	None stated
Integrated pump	Yes	Yes	Yes	No	N/A
Sample flow rate	1.4–3.0 L/min	1.0–3.5 L/min	2.83 L/min (fixed)	variable	N/A
Recommended flow velocity	N/A	N/A	N/A	N/A	3–40 m/s
Secondary Dilution required[d]	No	No	Yes	No	No
Operational temperature range[e]	0–50°C	-10–50°C	5–40°C	2–40°C	-40–60°C
Operational humidity range	0–95%	10–95%	20–95%	N/A	None stated–95%
Accessories	Impactors	Cyclones	N/A	Vacuum pump[f]	N/A

Continued on next page

Table S11 continued from previous page

	DustTrak II 8530	**pDR-1500**	**Particles Plus 8306**	**1405-D TEOM[a]**	**Sintrol S203**
Weight range[g]	1.6–2.5 kg	1.2 kg	1.0 kg	18 kg	1.5 kg
Dimensions	13.5×21.6×22.4 cm	18.1×14.3×8.4 cm	13.0×10.8×31.1 cm	43.2×48.3×75 cm	65.6×16.8×17.5 cm
External power	115–240 VAC	100–250 VAC	110–240 VAC	100–240 VAC	100–240 VAC
Battery power	Yes	Yes	Yes	No	No
Internal power	Removable Li-ion battery (up to 2)	4 AA alkaline batteries	Removable Li-ion battery	N/A	N/A
Continuous operation battery life	12 hours with 2 batteries 6 hours with 1 battery	$>$ 24 hours @ 1.2 L/min $>$ 6 hours @ 3.5 L/min	$>$ 10 hours	N/A	N/A
Sampling interval range	1 s–1 hr	1 s–1 hr	1 s–99 hr	10 s–1 hr	None stated
Zero calibration	Yes (user)	Yes (user)	Zero check only	Not available	Zero check only
Average setup time	$<$ 15 min	$<$ 15 min	$<$ 15 min	$>$ 1 hr	$<$ 15 min
Recommended factory calibration interval	1 yr	1 yr	1 yr	1 yr	Application dependent
Gravimetric correction	Required; integrated 37 mm filter	Required; integrated 37 mm filter	Required; external filter	Not required (direct mass)	N/A (TSP only)
Onboard gravimetric measurement	Yes (37 mm)	Yes (37 mm)	No	N/A	No
Cost per test filter replacement	$2.20	$2.20	N/A	$80 (requires two filters)	N/A
Sample downtime after filter change	0 min	0 min	N/A	20 min	N/A
Communication	USB, Ethernet, flash	USB, Ethernet, flash	USB, Ethernet, RS-485, RS-232, Wi-Fi, flash	RPComm software and RS-232, or flash	Analog 4-20 mA and RS-485
Internal storage capacity	60,000 samples	500,000 samples	45,000 samples	500,000 samples	PC log only
Manufacturer support available	Yes	Yes	Yes	No[h]	Yes
Approx. cost (USD)[i]	$8,600	$10,000	$5,000	$25,000–40,000	$5,000

[a] Measurement outputs without any accessories such as impactors or cyclones.
[b] Particle concentration range.
[c] Aerosol concentration range.
[d] Additional dilution required for measurement.
[e] Relative humidity, non-condensing.
[f] While the impactors and cyclones are optional accessories for the DustTrak and pDR, respectively, the vacuum pump is required for TEOM operation.
[g] The DustTrak can be operated with one, two, or zero batteries.
[h] Thermo Scientific will discontinue the 1405-D TEOM on June 30, 2026.
[i] Estimated 2026 USD.
[j] R^2 calculated from 10-s averaged data with regression through the origin. TEOM R^2 represents the best performing channel per phase.
[k] This range represents the best performing channel for each operational phase.

S-2.8. Parity and Bland–Altman plots

Because candidate instruments and the size-resolved reference were generally normalized to the 47 mm gravimetric filter mass for each burn phase, the mean bias in the Bland–Altman analysis is mathematically constrained near zero by design. Consequently, the mean bias line is omitted, allowing the limits of agreement and variance to evaluate real-time tracking dynamics and temporal scatter rather than absolute calibration offset. Exceptions occur during phases where gravimetric calibration factors were negative or undefined; in these cases, raw unscaled TEOM data are presented to preserve mass-loss dynamics, while Sintrol data are omitted where concentrations fell below its measurement limit.

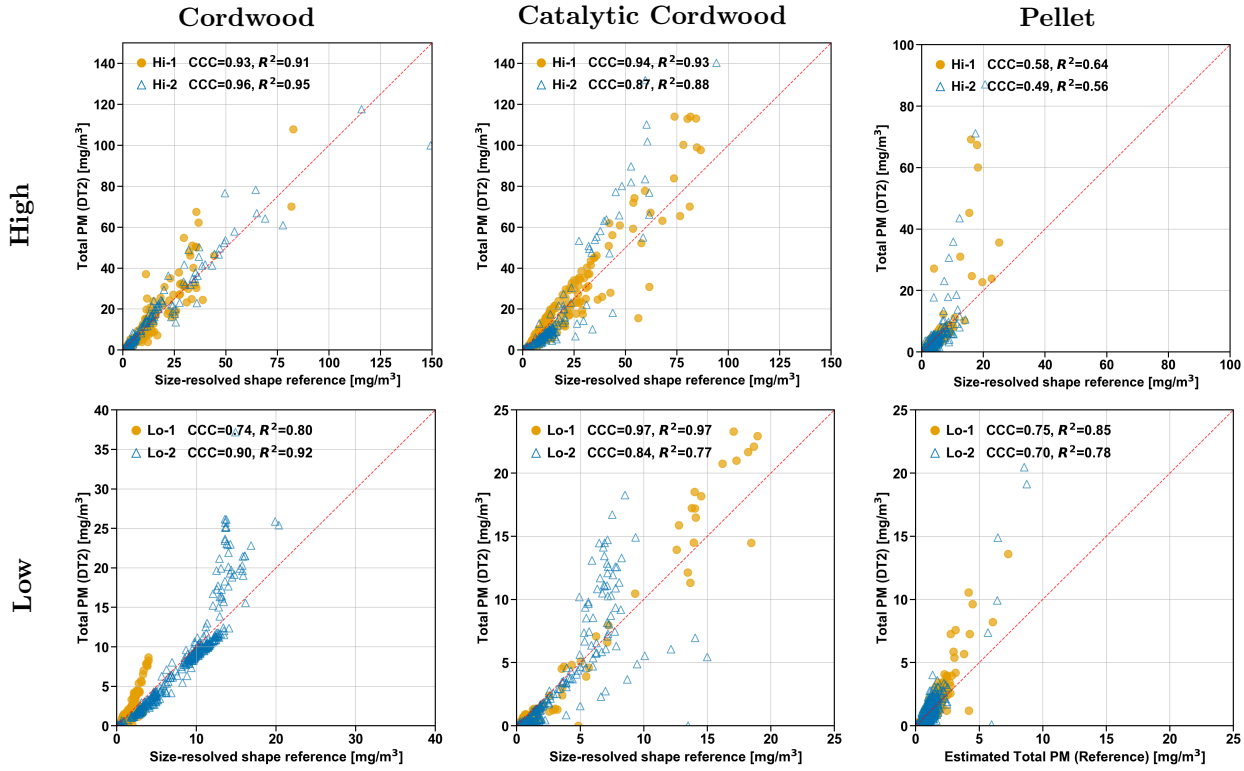


Figure S12: Parity plots of DustTrak II 8530 (DT2) measurements versus the size-resolved shape reference for three heater types (columns: Cordwood, Catalytic Cordwood, Pellet) and two operating phases (rows: High, Low). Circle and triangle markers denote the two replicate tests within each operating phase, and the red dashed line is the 1:1 reference. Inset values give Lin's concordance correlation coefficient (CCC) [40] and the coefficient of determination (R^2) from ordinary least squares regression. Instruments are scaled using phase-specific gravimetric correction factors shown in Table S8.

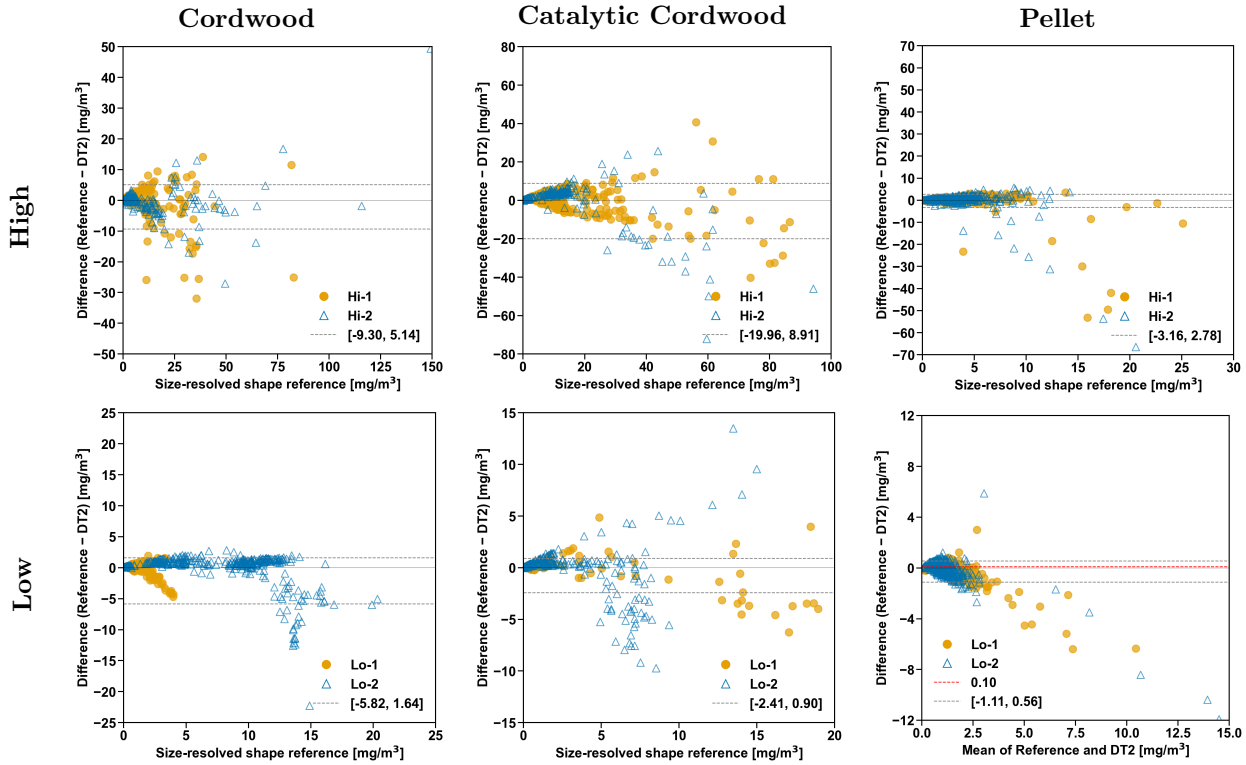


Figure S13: Bland–Altman plots of DustTrak II 8530 (DT2) measurements versus the size-resolved shape reference for three heater types (columns: Cordwood, Catalytic Cordwood, Pellet) and two operating phases (rows: High, Low). The gray dashed lines indicate the non-parametric 95% limits of agreement, calculated as the 2.5^{th} and 97.5^{th} percentiles of the pooled differences across both replicates within each panel. The solid black line marks zero difference. Circle and triangle markers denote the two replicate tests within each operating phase as in Figure S12. The mean bias is not shown since all instruments are scaled using phase-specific gravimetric correction factors (Table S8).

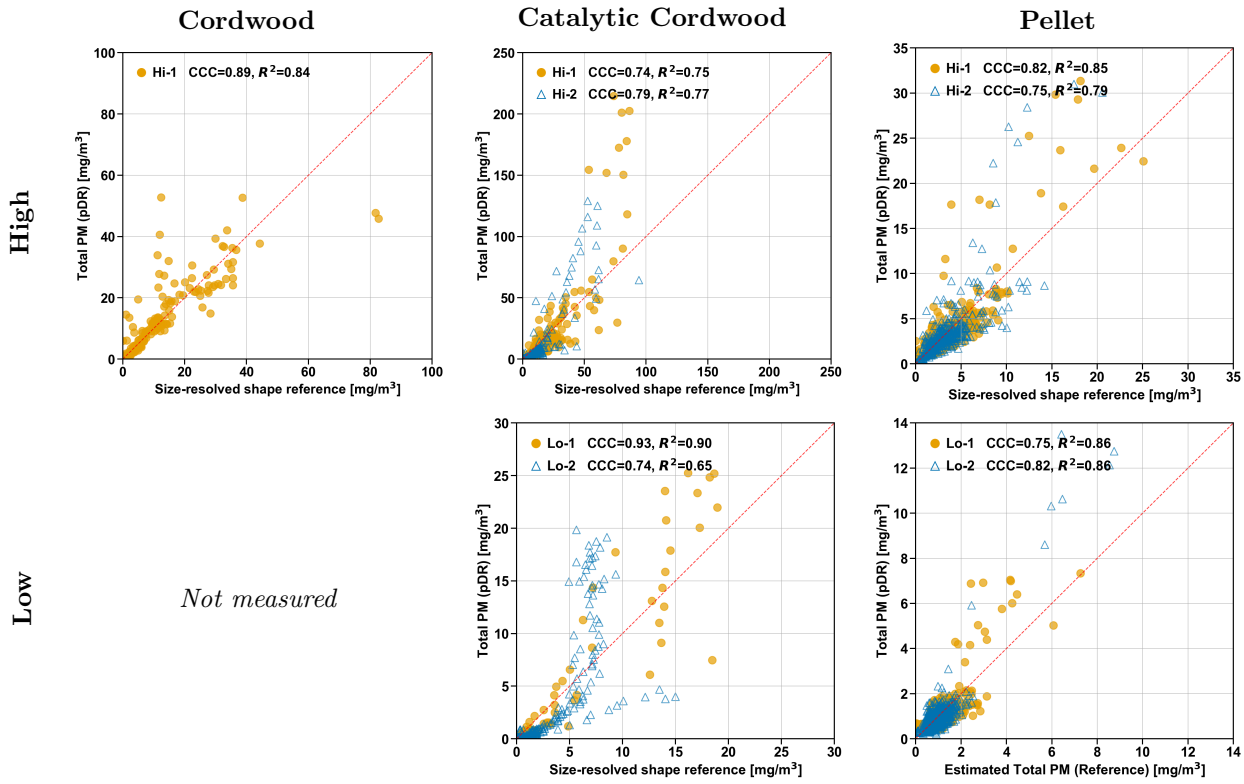


Figure S14: Parity plots of pDR-1500 measurements versus the size-resolved shape reference for three heater types (columns: Cordwood, Catalytic Cordwood, Pellet) and two operating phases (rows: High, Low). Circle and triangle markers denote the two replicate tests within each operating phase, and the red dashed line is the 1:1 reference. Inset values give Lin's concordance correlation coefficient (CCC) [40] and the coefficient of determination (R^2) from ordinary least squares regression. Instruments are scaled using phase-specific gravimetric correction factors shown in Table S8.

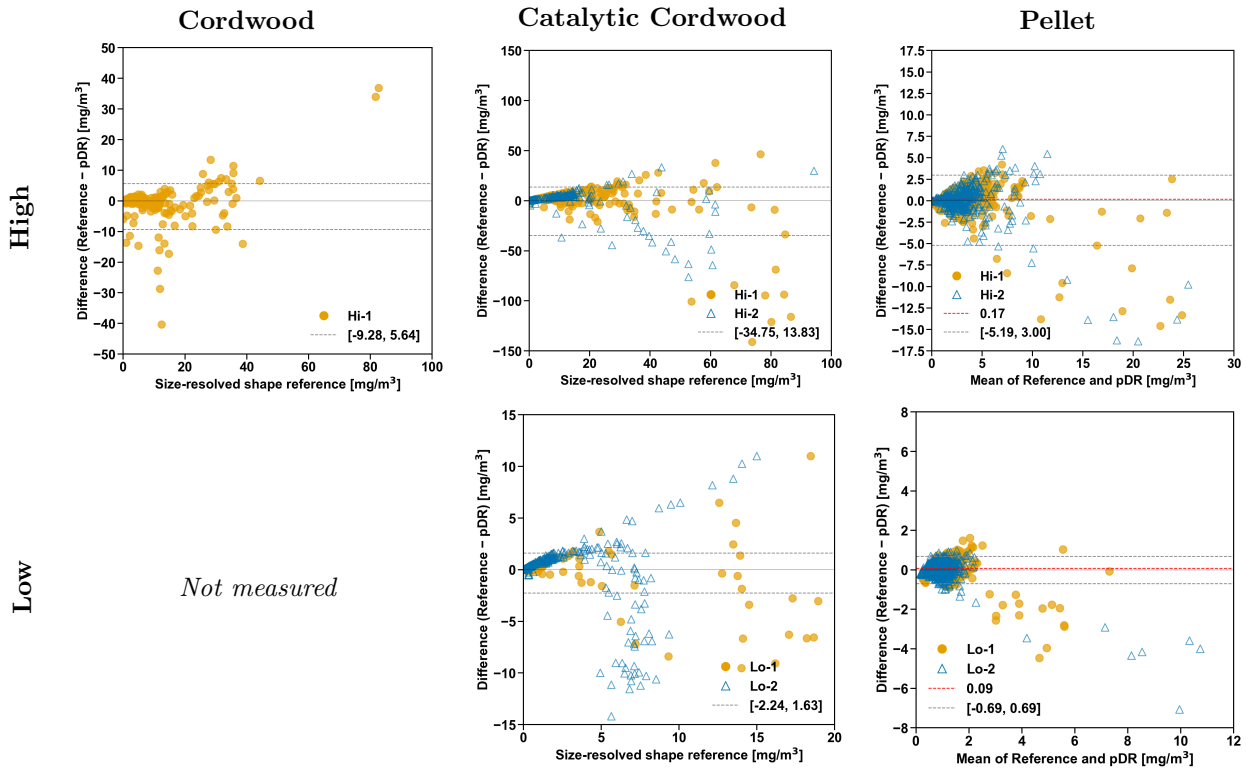


Figure S15: Bland–Altman plots of pDR-1500 measurements versus the size-resolved shape reference for three heater types (columns: Cordwood, Catalytic Cordwood, Pellet) and two operating phases (rows: High, Low). The gray dashed lines indicate the non-parametric 95% limits of agreement, calculated as the 2.5^{th} and 97.5^{th} percentiles of the pooled differences across both replicates within each panel. The solid black line marks zero difference. Circle and triangle markers denote the two replicate tests within each operating phase. A separate mean bias line is omitted since all instruments are scaled using phase-specific gravimetric correction factors (Table S8).

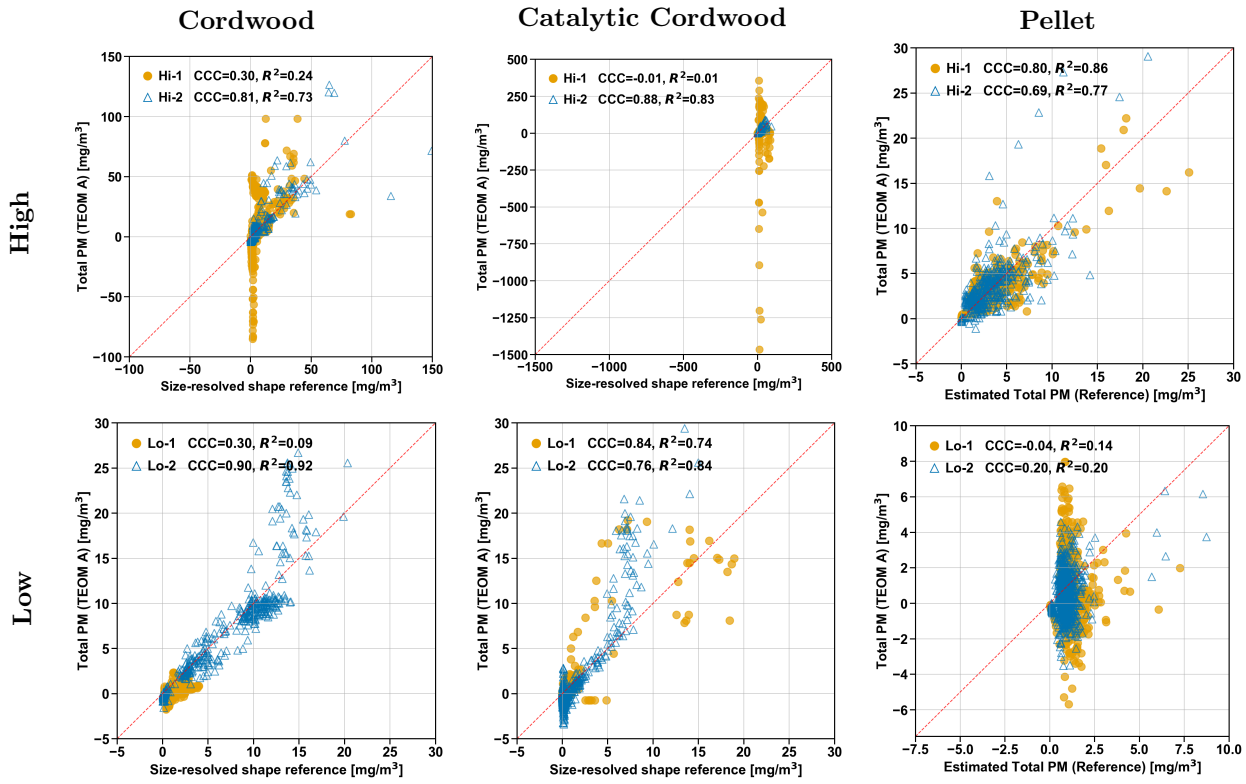


Figure S16: Parity plots of TEOM 1405D Channel A measurements versus the size-resolved shape reference for three heater types (columns: Cordwood, Catalytic Cordwood, Pellet) and two operating phases (rows: High, Low). Circle and triangle markers denote the two replicate tests within each operating phase, and the red dashed line is the 1:1 reference. Inset values give Lin's concordance correlation coefficient (CCC) [40] and the coefficient of determination (R^2) from ordinary least squares regression. Instruments are scaled using phase-specific gravimetric correction factors (Table S8), except during the Cordwood Low-1 and Catalytic Cordwood High-1 test phases. For these two phases, raw unscaled TEOM Channel A data are presented to preserve authentic mass-loss dynamics, as net negative mass measurements throughout the phase yielded a negative correction factor.

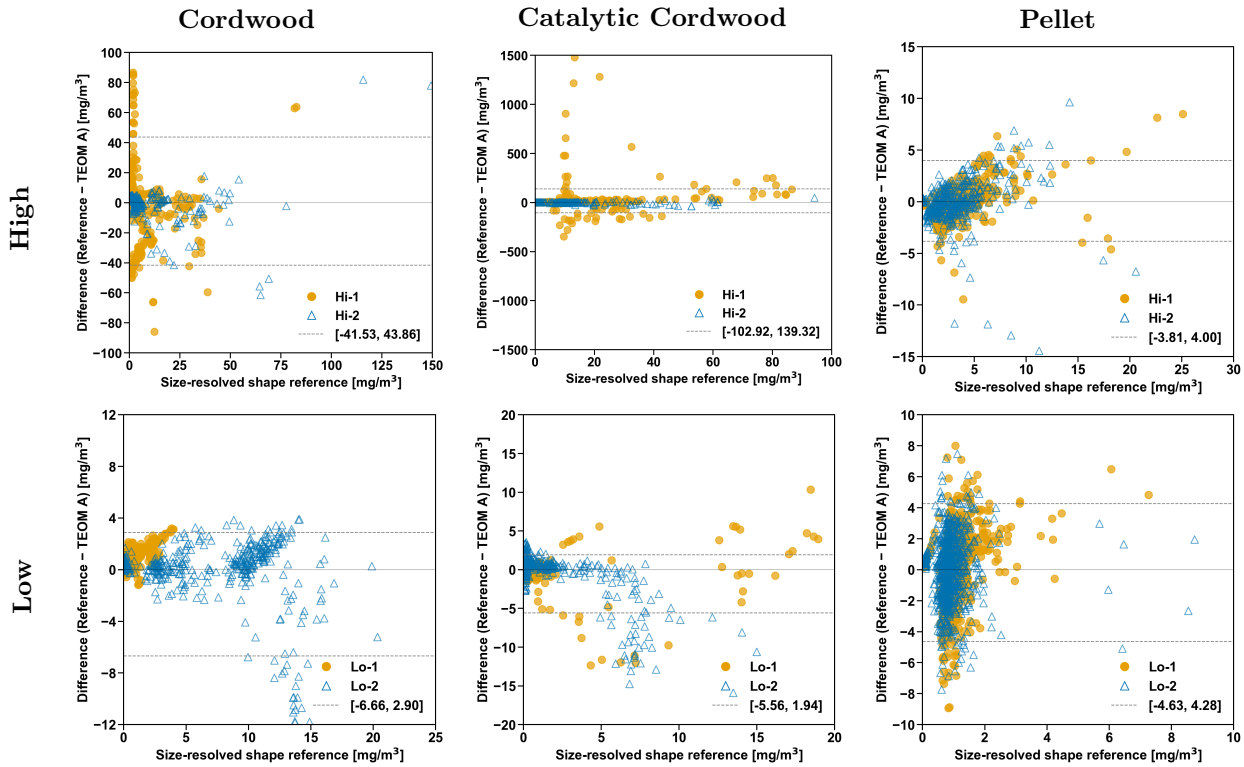


Figure S17: Bland–Altman plots of TEOM 1405D Channel A measurements versus the size-resolved shape reference for three heater types (columns: Cordwood, Catalytic Cordwood, Pellet) and two operating phases (rows: High, Low). The gray dashed lines indicate the non-parametric 95% limits of agreement, calculated as the 2.5^{th} and 97.5^{th} percentiles of the pooled differences across both replicates within each panel. The solid black line marks zero difference. Circle and triangle markers denote the two replicate tests within each operating phase. A separate mean bias line is omitted since all instruments are scaled using phase-specific gravimetric correction factors (Table S8). During the Cordwood Low-1 and Catalytic Cordwood High-1 test phases, raw unscaled TEOM Channel A data are presented to preserve authentic mass-loss dynamics, as net negative mass measurements throughout the phase yielded a negative correction factor.

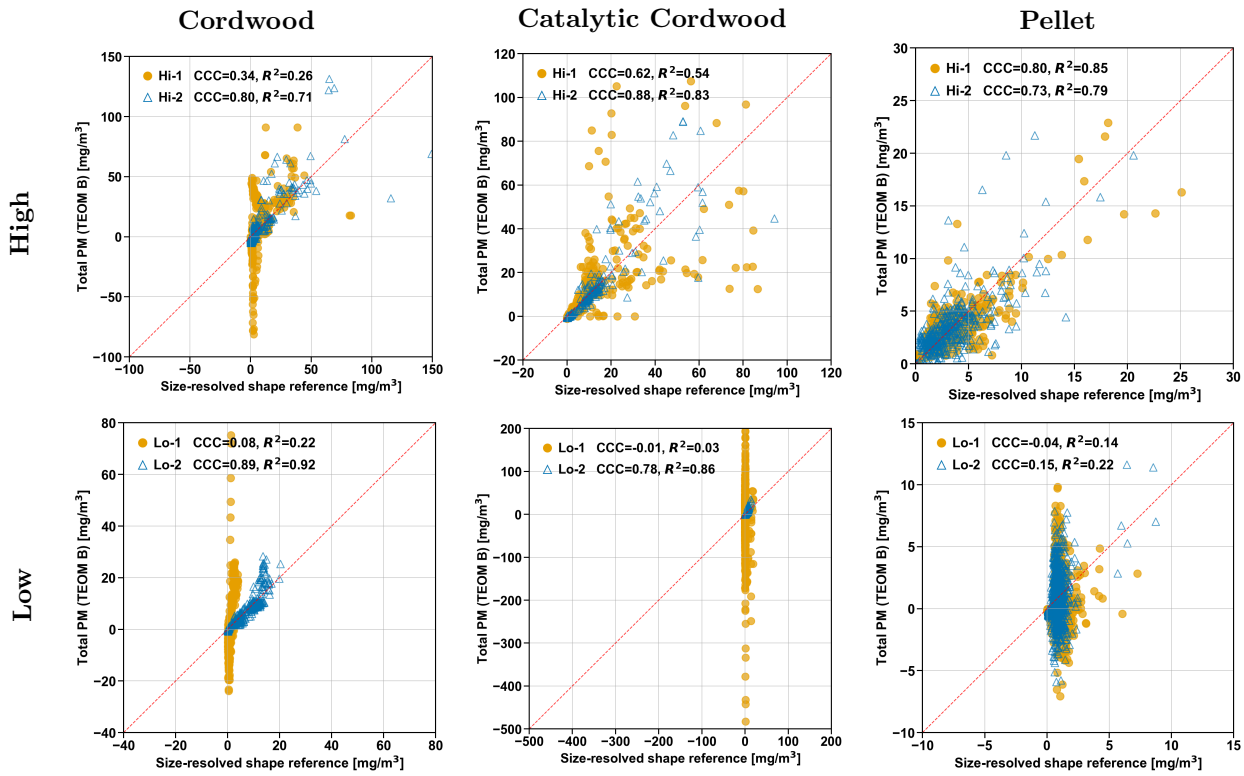


Figure S18: Parity plots of TEOM 1405D Channel B measurements versus the size-resolved shape reference for three heater types (columns: Cordwood, Catalytic Cordwood, Pellet) and two operating phases (rows: High, Low). Circle and triangle markers denote the two replicate tests within each operating phase, and the red dashed line is the 1:1 reference. Inset values give Lin's concordance correlation coefficient (CCC) [40] and the coefficient of determination (R^2) from ordinary least squares regression. Instruments are scaled using phase-specific gravimetric correction factors (Table S8), except during the Catalytic Cordwood Low-1 test phase. For this phase, raw unscaled TEOM Channel B data are presented to preserve authentic mass-loss dynamics, as net negative mass measurements throughout the phase yielded a negative correction factor.

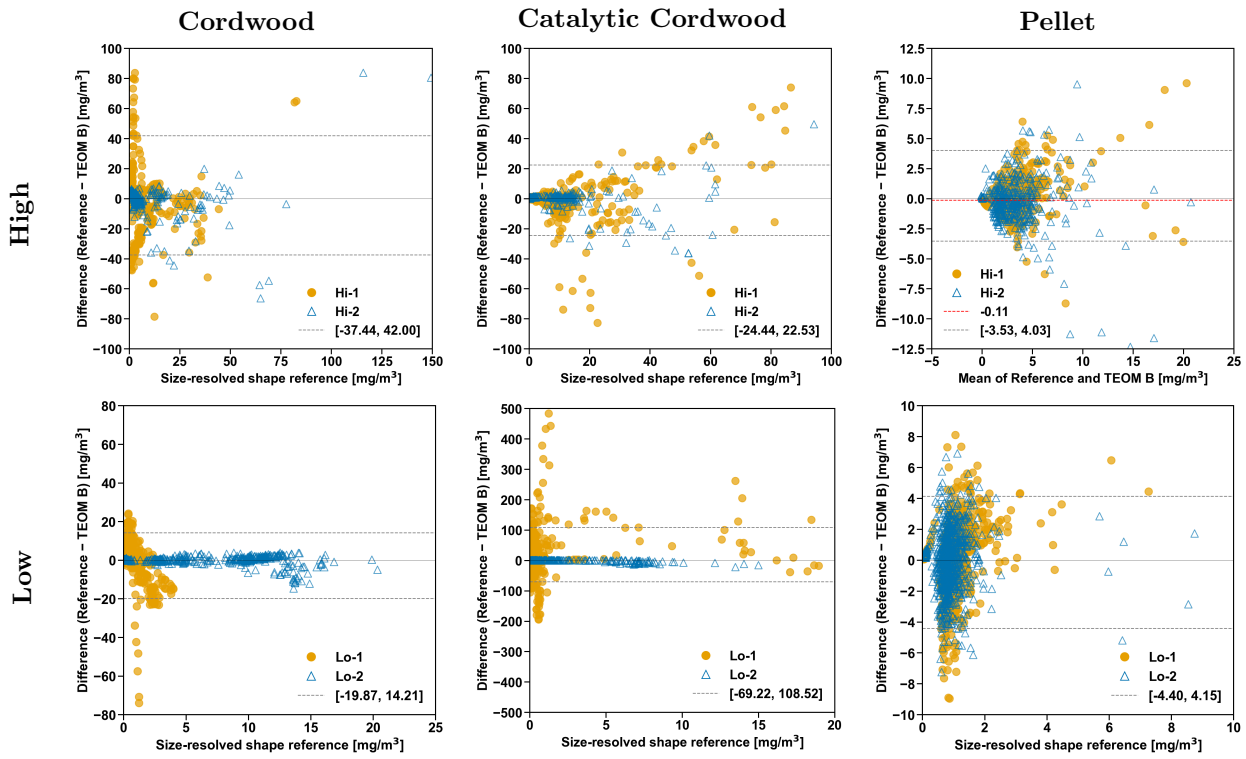


Figure S19: Bland–Altman plots of TEOM 1405D Channel B measurements versus the size-resolved shape reference for three heater types (columns: Cordwood, Catalytic Cordwood, Pellet) and two operating phases (rows: High, Low). The gray dashed lines indicate the non-parametric 95% limits of agreement, calculated as the 2.5^{th} and 97.5^{th} percentiles of the pooled differences across both replicates within each panel. The solid black line marks zero difference. Circle and triangle markers denote the two replicate tests within each operating phase. A separate mean bias line is omitted since all instruments are scaled using phase-specific gravimetric correction factors (Table S8). During the Catalytic Cordwood Low-1 phase, raw unscaled TEOM Channel B data are presented to preserve authentic mass-loss dynamics, as net negative mass measurements throughout the phase yielded a negative correction factor.

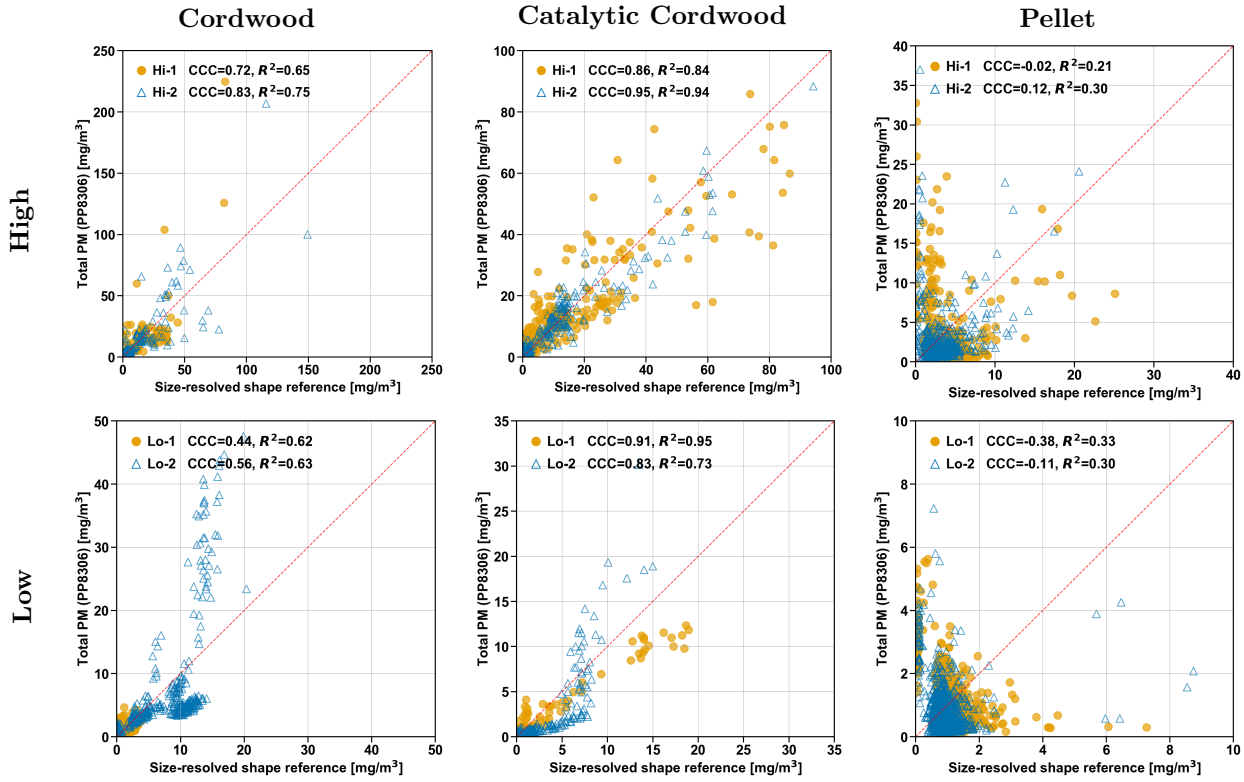


Figure S20: Parity plots of PP8306 measurements versus the size-resolved shape reference for three heater types (columns: Cordwood, Catalytic Cordwood, Pellet) and two operating phases (rows: High, Low). Circle and triangle markers denote the two replicate tests within each operating phase, and the red dashed line is the 1:1 reference. Inset values give Lin's concordance correlation coefficient (CCC) [40] and the coefficient of determination (R^2) from ordinary least squares regression. Instruments are scaled using phase-specific gravimetric correction factors shown in Table S8.

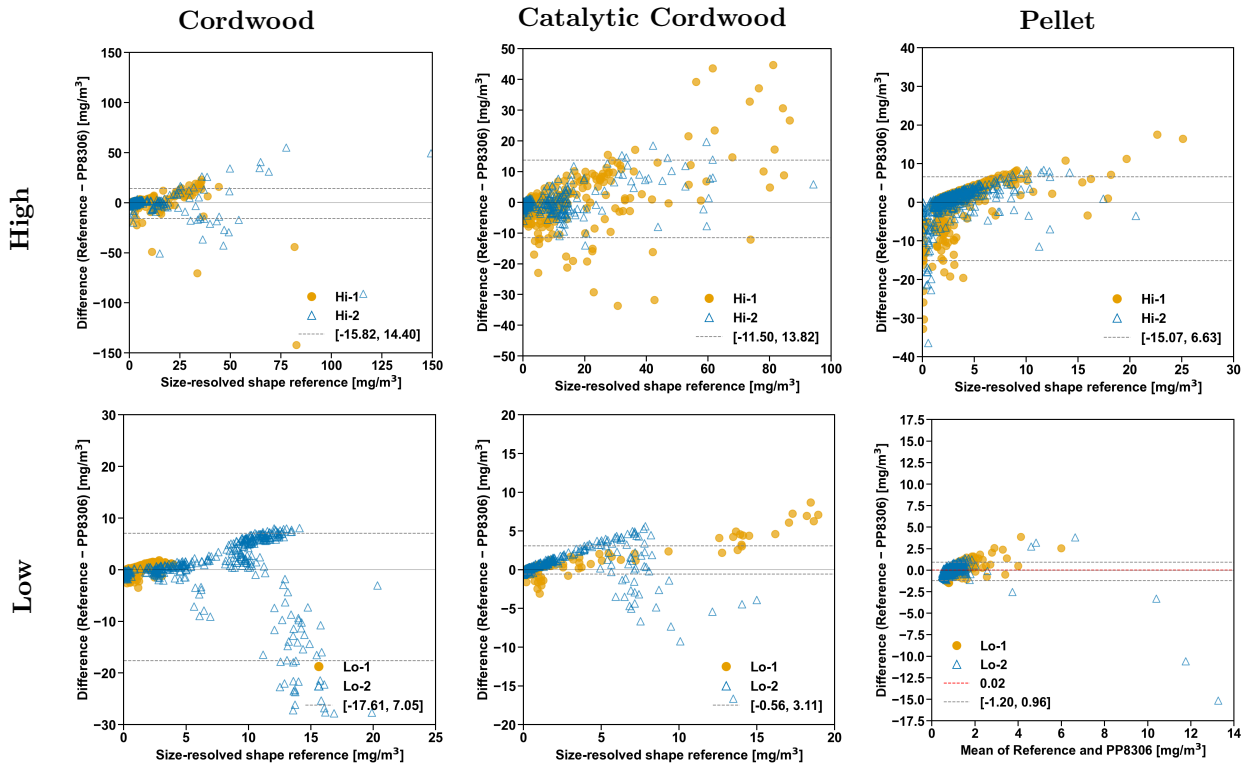


Figure S21: Bland–Altman plots of PP8306 measurements versus the size-resolved shape reference for three heater types (columns: Cordwood, Catalytic Cordwood, Pellet) and two operating phases (rows: High, Low). The gray dashed lines indicate the non-parametric 95% limits of agreement, calculated as the 2.5^{th} and 97.5^{th} percentiles of the pooled differences across both replicates within each panel. The solid black line marks zero difference. Circle and triangle markers denote the two replicate tests within each operating phase. A separate mean bias line is omitted since all instruments are scaled using phase-specific gravimetric correction factors (Table S8).

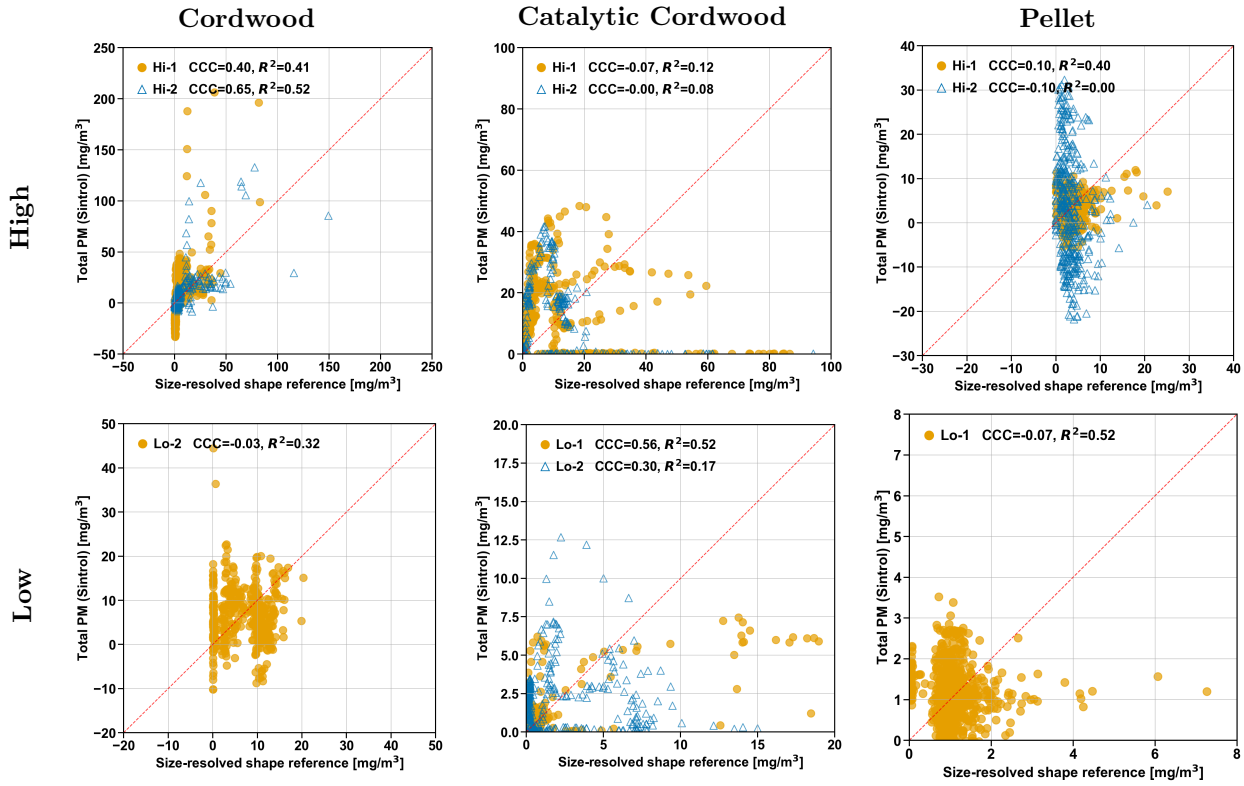


Figure S22: Parity plots of Sintrol S203 measurements versus the size-resolved shape reference for three heater types (columns: Cordwood, Catalytic Cordwood, Pellet) and two operating phases (rows: High, Low). Circle and triangle markers denote the two replicate tests within each operating phase, and the red dashed line is the 1:1 reference. Inset values give Lin's concordance correlation coefficient (CCC) [40] and the coefficient of determination (R^2) from ordinary least squares regression. Instruments are scaled using phase-specific gravimetric correction factors (Table S8), except during the Cordwood Low-1 and Pellet Low-2 test phases. Sintrol data are omitted for these phases as PM concentrations were below the instrument's measurement limit, yielding an undefined gravimetric calibration factor.

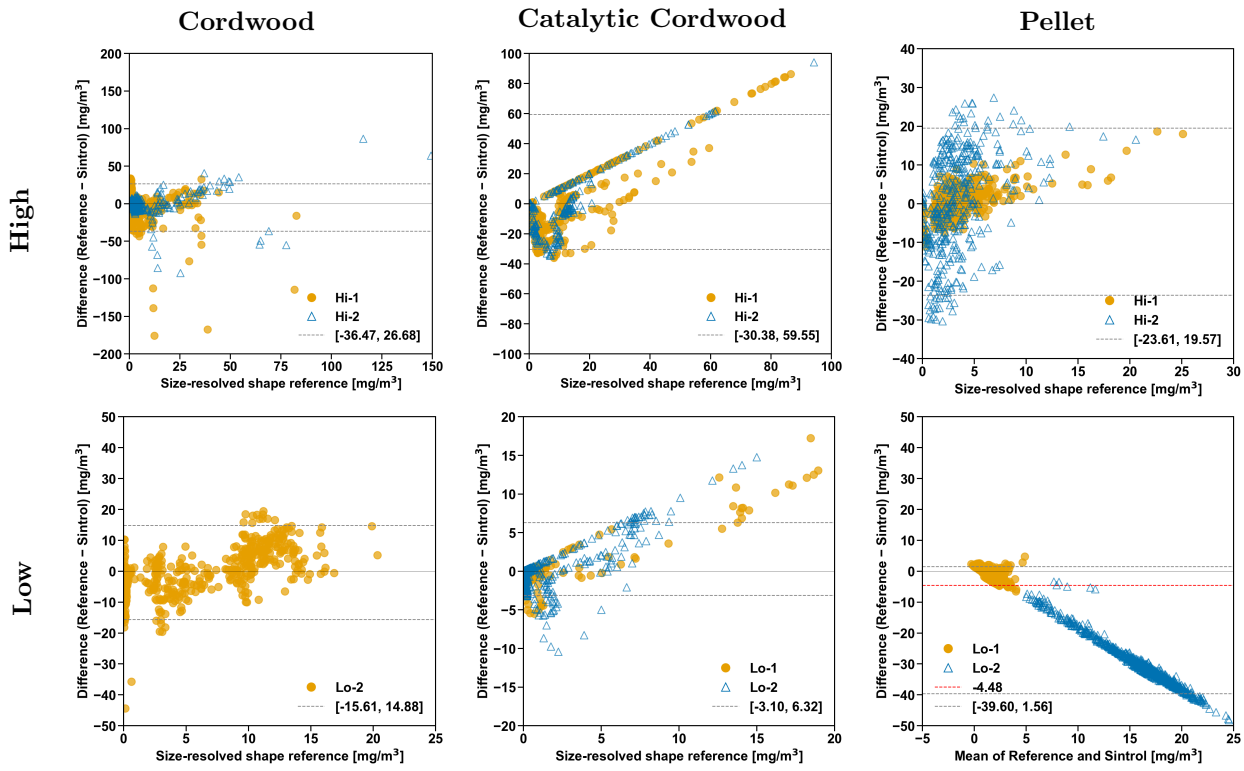


Figure S23: Bland–Altman plots of Sintrol S203 measurements versus the size-resolved shape reference for three heater types (columns: Cordwood, Catalytic Cordwood, Pellet) and two operating phases (rows: High, Low). The gray dashed lines indicate the non-parametric 95% limits of agreement, calculated as the 2.5^{th} and 97.5^{th} percentiles of the pooled differences across both replicates within each panel. The solid black line marks zero difference. Circle and triangle markers denote the two replicate tests within each operating phase. A separate mean bias line is omitted since all instruments are scaled using phase-specific gravimetric correction factors (Table S8). During the Cordwood Low-1 and Pellet Low-2 test phases, Sintrol data are omitted because PM concentrations were below the instrument's measurement limit, yielding an undefined gravimetric calibration factor.